AFRL-RQ-WP-TR-2016-0020

ADAPTIVE ORIGAMI FOR EFFICIENTLY FOLDED STRUCTURES

James J. Joo and Greg Reich

Design and Analysis Branch
Aerospace Vehicles Division

Kazuko Fuchi

Wright State Research Institute

FEBRUARY 2016
Final Report

AIR FORCE RESEARCH LABORATORY
AEROSPACE SYSTEMS DIRECTORATE
WRIGHT-PATTERSON AIR FORCE BASE, OH 45433-7541
AIR FORCE MATERIEL COMMAND
UNITED STATES AIR FORCE

NOTICE AND SIGNATURE PAGE

Using Government drawings, specifications, or other data included in this document for any purpose other than Government procurement does not in any way obligate the U.S. Government. The fact that the Government formulated or supplied the drawings, specifications, or other data does not license the holder or any other person or corporation; or convey any rights or permission to manufacture, use, or sell any patented invention that may relate to them.

This report was cleared for public release by the USAF 88th Air Base Wing (88 ABW) Public Affairs Office (PAO) and is available to the general public, including foreign nationals.

Copies may be obtained from the Defense Technical Information Center (DTIC) (http://www.dtic.mil).

AFRL-RQ-WP-TR-2016-0020 HAS BEEN REVIEWED AND IS APPROVED FOR PUBLICATION IN ACCORDANCE WITH ASSIGNED DISTRIBUTION STATEMENT.

*//Signature//
JAMES J. JOO
Program Manager
Design and Analysis Branch
Aerospace Vehicles Division

//Signature//
CHRISTOPHER D. TERPENING, Chief
Design and Analysis Branch
Aerospace Vehicles Division

//Signature//
PHILIP S. BERAN
Branch Technical Advisor
Aerospace Vehicles Division
Aerospace Systems Directorate

This report is published in the interest of scientific and technical information exchange and its publication does not constitute the Government's approval or disapproval of its ideas or findings.

*Disseminated copies will show "//Signature//" stamped or typed above the signature blocks.

REPORT DOCUMENTATION PAGE

Form Approved
OMB No. 0704-0188

1. REPORT DATE *(DD-MM-YY)*	2. REPORT TYPE	3. DATES COVERED *(From - To)*
February 2016	Final	03 December 2012 – 31 January 2016

4. TITLE AND SUBTITLE
ADAPTIVE ORIGAMI FOR EFFICIENTLY FOLDED STRUCTURES

5a. CONTRACT NUMBER
In-house

5b. GRANT NUMBER

5c. PROGRAM ELEMENT NUMBER
61102F

6. AUTHOR(S)
James J. Joo and Greg Reich (AFRL/RQVC)
Kazuko Fuchi (Wright State Research Institute)

5d. PROJECT NUMBER
3002

5e. TASK NUMBER

5f. WORK UNIT NUMBER
Q12C

7. PERFORMING ORGANIZATION NAME(S) AND ADDRESS(ES)
Design and Analysis Branch (AFRL/RQVC)
Aerospace Vehicles Division
Air Force Research Laboratory, Aerospace Systems Directorate
Wright-Patterson Air Force Base, OH 45433-7541
Air Force Materiel Command, United States Air Force

Wright State Research Institute
4035 Colonel Glenn Hwy
Beavercreek, OH 45431

8. PERFORMING ORGANIZATION REPORT NUMBER
AFRL-RQ-WP-TR-2016-0020

9. SPONSORING/MONITORING AGENCY NAME(S) AND ADDRESS(ES)
Air Force Research Laboratory
Aerospace Systems Directorate
Wright-Patterson Air Force Base, OH 45433-7541
Air Force Materiel Command
United States Air Force

10. SPONSORING/MONITORING AGENCY ACRONYM(S)
AFRL/RQVC

11. SPONSORING/MONITORING AGENCY REPORT NUMBER(S)
AFRL-RQ-WP-TR-2016-0020

12. DISTRIBUTION/AVAILABILITY STATEMENT
Approved for public release; distribution unlimited.

13. SUPPLEMENTARY NOTES
PA Case Number: 88ABW-2016-0843; Clearance Date: 25 February 2016.

14. ABSTRACT
Origami, the art of paper folding, transforms a flat sheet into complex, active or passive art using sequential mathematically defined actions. The goal of this research is to develop methodologies and toolsets necessary to integrate physics-based considerations into these procedures, and thus afford a new design strategy to solve aerospace and challenges with mechanically relevant performance criteria that are faced by Air Force personnel.

15. SUBJECT TERMS
origami, topology optimization, folding, Truss model, LCE

16. SECURITY CLASSIFICATION OF:			17. LIMITATION OF ABSTRACT:	18. NUMBER OF PAGES	19a. NAME OF RESPONSIBLE PERSON (Monitor)
a. REPORT	b. ABSTRACT	c. THIS PAGE			James J. Joo
Unclassified	Unclassified	Unclassified	SAR	47	19b. TELEPHONE NUMBER *(Include Area Code)* N/A

Table of Contents

Section **Page**

List of Figures

Figure **Page**

Acknowledgements

This work was supported by the Air Force Office of Scientific Research (AFOSR) funding, LRIR 13RQ02COR. We gratefully acknowledge Joycelynn Harrison and David Stargel for their enthusiasm and support of the project.

1. Summary

Origami, the art of paper folding, transforms a flat sheet into complex, active or passive art using sequential, mathematically defined actions. The goal of this research is to develop methodologies and toolsets necessary to integrate physics-based considerations into these procedures, and thus afford a new design strategy to solve aerospace and airmen challenges with mechanically relevant performance criteria. The key objectives are:

- Integrate a physics-based origami analysis within an optimization algorithm to design and evaluate active and passive origami structures with respect to functional performance criteria beyond geometry
- Identify material parameters to quantitatively compare fold performance of engineering materials
- Develop a design methodology to optimize the programming and distribution of stimuli responsive material to achieve self-folding origami structures
- Establish a U.S.-based community focused on developing origami-based technology for aerospace opportunities, and training students in this highly multidisciplinary (optimization, structure, materials) field.

These objectives enable the impact of origami concepts to AF applications to be evaluated. These applications include optimal packaging of solar cell panels, reconfigurable structures, advanced structural/material concepts, sensor platforms, and remotely actuated structures.

2. Introduction

2.1 Background

The appeal of origami and programmed folding is its simplicity, versatility, and ability to harness the multitude of 2D patterning techniques (e.g., inkjet, screen printing, lithography) to convert surface patterns on substrates into stable 3D objects. The design and fabrication of structures based on folding/unfolding of 2D sheets is a novel paradigm that will deliver unprecedented function with relevance in many AFRL science and technology (S&T) priority areas. The Flexible Electronic Materials and Devices research team has specific interest in the novel form factors and 2D fabrication capability of origami design concepts. Initial FLEX team demonstrations of an origami solar array and an origami concept for a tunable frequency selective surface (FSS) underscore the potential of an origami approach. The potential for origami to innovate electronic devices is a key motivating factor behind AFOSR's upcoming 2016 Multidisciplinary University Research Initiative entitled "4D Electromagnetic Origami." The origami team has also collaborated with the AFRL Cooperative Research and Development Fund program on liquid metal to develop additional strategies for electromagnetic reconfiguration and conductivity across fold lines. Broader impacts for AF include lightweight structural designs for *weight savings to increased system capabilities*, energy harvesting systems for *energy efficiency and power*, active and passive damping for *sustainment*, un-foldable air foils for precision airdrop and *autonomy*, single degree of freedom actuators to achieve vortex generation for *aerodynamic control*, threat-triggered hardening of structures and sensors for *operation in contested environment*, and deployment/tuning of antennas and other sensors for *surveillance and communications*. Additionally, the reconfigurable nature of an active origami system multiplies the potential value of the technology, ranging from a logistic standpoint: ***being able to replace a number of different parts***, to an operational one: ***being able to carry packaged systems for later deployment of multifunctional systems***.

2.2 Notable Highlights

Our AFRL-based multidisciplinary team leverage expertise in mathematics; mechanics; structural optimization; material processing and fabrication. The most impactful successes of the LRIR include:

- Comprehensive mechanical analysis toolsets with full integration into the design optimizer: We were the first to develop a physics-based, computational origami design tool that integrates mechanics analysis into crease pattern design optimization. Three mechanical analysis tools were developed for increasingly complex deformation regimes: 1) truss elements were developed for efficient analysis of intermediate fold angle and nearly rigid problems (truss design code publically released in 2015, 50+ downloads); 2) frame elements for larger fold and compliant fold line problems; and 3) brick finite elements (FE) with anisotropic director profiling for modeling liquid crystal elastomers (LCE). A gradient-based optimizer was integrated with these tools to design an actuator, identify the fold direction for maximal in-plane compression, and determine the LCE director profile to create a hinge (5 publications).
- Origami patterns for actuation, networking and tunable dynamic response: By phrasing action origami design as an optimization problem of distributing fold and facet stiffness, we transformed a traditionally artistic process to an engineering problem of material distribution.

The capability of the design optimization approach was demonstrated through 1) robust rediscoveries of known action origami designs, 2) the discovery of new origami-based mechanism designs, 3) the design of optimal network of actuators, and 4) providing insight into the role of design problem symmetry on the optimized result.

- Material failure behavior underlying fold performance: By defining terminology with respect to mechanical characteristics of an engineering material, the definition of fold bend, and crease was established. Crease mechanics is an enabling knowledge base for flexible hybrid electronics, for which criteria for flexible substrate selection and foldable materials are needed. Mechanically relevant metrics for folding were identified and quantified via a custom crease test apparatus, including residual fold angle, fold angle relaxation, dissipated mechanical energy, and size of the surface plastic zone. For analysis, we were the first to develop a bending mechanics model with material specific data that predicts residual fold angle. Overall, the test enables direct measurement of critical parameters needed for integrating mechanics into origami design (published at SMASIS 2014, 1st place in the Midwest and 2nd place in the National 2014 SAMPE student research symposium).
- Design of self-folding and programmable material systems: Nafion SMP Programming: To integrate active materials into origami, mechanical analysis and optimization tools where applied to the fabrication of the fundamental origami motif: a hinge. The team was the first to demonstrate a general strategy for shape reprogramming in a polymer such as Nafion, where prescribed 3D geometric information can be encoded as a spatially patterned composite of discrete shape-memory and locked-shape-memory phases via a reversible localized deprotonation mechanism (Advanced Materials 2014 cover).
- LCE Design: The team was the first to enable detailed hinge design in optically and thermally triggered shape-changing polymer films by using our mechanical and design optimization methods to determine the optimal point-by-point LCE director profile for reversible folding. This work demonstrated that origami design concepts can be leveraged to program material microstructure, highlighting the relevance of an origami design motif over a broad range of length scales. Additive manufacturing techniques were also leveraged to localize the LCE activation. An electro-thermal heating approach significantly broadens the control and range of applications that LCE origami can impact.
- Origami for Electromagnetic (EM) Tuning: We have extended the performance criteria for origami to include relevant EM features, such as the frequency and polarization response of the scattering parameters of radio frequency (RF) components. A computational survey of common FSS designs folded into known origami tessellations demonstrated that modest folding could induce resonance frequency shifts. The findings points to EM origami as a viable approach for spatial tuning of RF devices.
- Creating a U.S. Origami Engineering community. To complement these efforts, we created and hosted the initial ODESSEI Origami Workshop, actively supported NSF/AFOSR evaluation panels (FY12-13), held six on-site technical exchange events with ODESSI-EFRI awardees, including a student exchange, and led or co-organized 7 workshops at national and international meetings. During FY13-FY15, Ten peer-reviewed papers were accepted for publication and one was submitted for review. Three patents were acquired and 25 research presentations were given, where 11 were invited.

3. Development of Origami Mechanics Design Tools

Origami provides a strategy for mapping between two or more geometric states through a series of fold operations. However, designing origami structures presents several challenges:

- What is the optimal pattern of fold lines to achieve a target folded shape?
- What is the optimal fold direction?
- What is the optimal distribution of fold stiffness to minimize the required input energy or bias the direction of folding under complex loading?
- How can facet and fold line compliance be used to create dissipative structures?

Geometry-based design tools, such as Treemaker and Rigid Origami Simulator, address some of these challenges, i.e., finding the 2D pattern of fold lines required to achieve a target 3D shape. However, these tools do not evaluate mechanical metrics such as stiffness and input energy, but instead assume rigid origami with inextensible fold lines and perfect hinges. More importantly, geometric approaches assume the target shape is known, which is typically not the case for design criteria based on mechanical function. To address these challenges, mechanical analysis toolsets were developed and integrated into a gradient-based optimization algorithm to create a design tool for origami structures with mechanically relevant functions.

3.1 Truss Model

Design optimization inherently involves a tradeoff between modeling complexity and computational expense. Truss elements were developed for computationally efficient analysis of intermediate ranges of fold angles ($< 30^{\circ}$) and nearly rigid problems. All truss elements in the reference grid have stiffness associated with elongation, and all truss elements within the interior (non-edge) of the grid have an additional stiffness associated with changes in dihedral angles defined by local triads of truss members. The modified truss model was originally developed to characterize the mechanics of origami tessellations [1] and has been employed in this tool for its computational efficiency for small displacement design problems. The elemental stiffness matrix $\boldsymbol{K}$ of the modified truss has the following form,

$$\boldsymbol{K} = \begin{bmatrix} \boldsymbol{C} \\ \boldsymbol{J} \end{bmatrix}^T \begin{bmatrix} \boldsymbol{G} & 0 \\ 0 & \boldsymbol{G_J} \end{bmatrix} \begin{bmatrix} \boldsymbol{C} \\ \boldsymbol{J} \end{bmatrix} = \boldsymbol{C}^T \boldsymbol{G} \boldsymbol{C} + \boldsymbol{J}^T \boldsymbol{G_J} \boldsymbol{J}$$

where $\boldsymbol{C}$ and $\boldsymbol{J}$ refer to the compatibility matrix and the Jacobian of the dihedral angles with respect to nodal displacements. The material properties pertaining to bar elongation and folding are described through $\boldsymbol{G}$ and $\boldsymbol{G_J}$, respectively. The advantage of this formulation for optimization is that fold stiffness $\boldsymbol{G_J}$ may be sufficiently scaled to effectively add or remove fold lines. Crease pattern designs are described through distributions of fold stiffness G_J^k within a reference crease pattern. The design variable α_k is used to specify the folding property of segment k as

$$G_J^k = 10^{\alpha^0 + \alpha_k(\alpha^1 - \alpha^0)}$$

with constants $\alpha^0 = 2$ and $\alpha^1 = 8$. G_J^k takes a value between the prescribed fold stiffness 10^{α^0} and facet bending stiffness 10^{α^1} for each fold line k. The mechanical boundary conditions employed in this study include fixed nodes (denoted as green triangles) and point loads (denoted as red squares). The design objective is to maximize the displacement of selected nodes (blue circles), which can be represented as a weighted sum. A constraint on the number of fold lines is

used to simplify the design solution and better identify the key topologies responsible for actuation. The allowable fold line fraction is defined as $l_0 = 1 - v_0$, where $0 \leq v_0 \leq 1$. The fold stiffness optimization problem may be represented as follows:

Find $\alpha_1, \alpha_2, \cdots, \alpha_{Nf}$ that

Maximize $f = \boldsymbol{c}^T \boldsymbol{u}$ (output deflection)

Subject to $g = v_0 - \frac{1}{N_f} \sum_{k=1}^{N_f} \alpha_k \leq 0$

$0 \leq \alpha_k \leq 1 \; \forall \; k = 1,2, \cdots, N_f$

and is schematically represented by the flowchart in Figure 1(A). Fold stiffness optimization will be repeated for the same design problem on a series of refined and topologically distinct reference grids. The method of moving asymptotes (MMA) [2], a gradient-based optimization technique, is used for the fold stiffness optimization. Convergence is based on the 1st order Karush-Kuhn-Tucker (KKT) optimality condition.

3.2 Design of 2D-to-3D Actuating Mechanisms

Actuating structures are fundamental to AF application of morphing wings, remote sensing, precision tuning and other areas. The design challenge of this study was to determine the optimal fold pattern for an actuating mechanism from the initial flat state. As shown in Figure 1B, a set of interior grid nodes were fixed (green arrows), two loads (red squares) were applied at the boundary of the grid perpendicular to the fixed node axis and the performance objective was to maximize the out-of-plane displacement of the boundary nodes colinear with fixed axis (blue nodes). The optimal crease pattern for this problem and reference grid is shown in Figure 1C in the deformed configuration, which is equivalent to the known action origami design called Chomper (Figure 1D). The result illustrates a mechanism that achieves 3D performance, but is designed within a 2D design space, leveraging one of the most relevant characteristics of origami. One of the limitations of starting with a reference grid of fold lines is that the design space is constrained a priori. As seen in Figure 1E, the chomper solution can be recovered from several different starting topologies when an appropriate constraint on the number allowed fold lines is applied. Various reference patterns were studied, as shown in Figure 1E; results converge to the same solution when matching the problem specifications, indicating the robustness of the optimization algorithm. However, to better understand the coupling of the reference grid with the design space, the following sections investigate the effect of grid density and nodal connectivity on the 2D to 3D actuator performance.

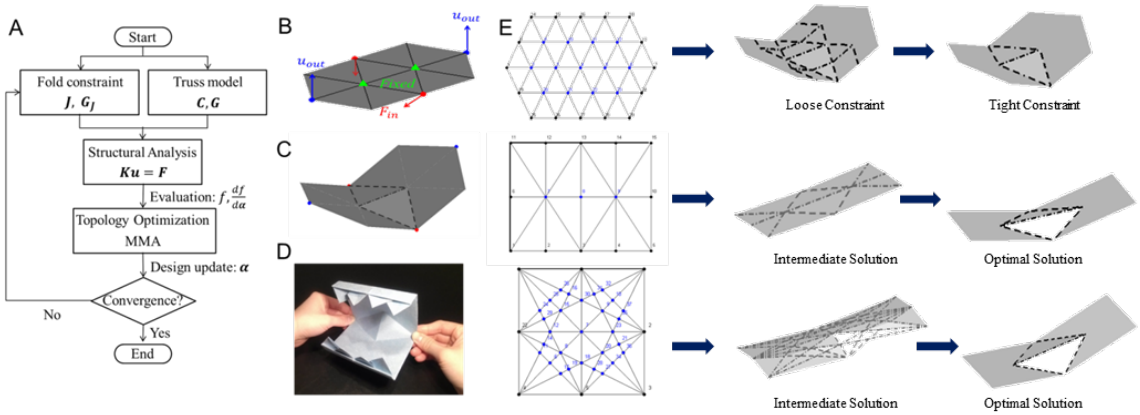

Figure 1: Mechanism Design through Topology Optimization of Origami Crease Pattern

3.3 Role of Mesh Refinement in Actuation Mechanisms

One of the challenges of topology optimization is determining how the grid choice may constrain the design space and limit the achievable performance. The aim of this study is to characterize this grid effect through two different strategies. First, an actuator design problem will be solved on a series of reference grids with increased degrees of mesh refinement. In this way, more design freedom is introduced through the addition of more nodes and potential fold lines in the grid. Second, after identifying an optimal solution on the refined grids, the position of the nodes associated with fold lines will be optimized to identify additional improvements to the actuator design. Optimization of nodal positions enables a specific enhancement of design freedom, whereas the mesh refinement approaches introduces a general enhancement of design freedom. The fold stiffness and node position optimization are combined in this study to identify fundamental topologies for actuation and to study the consolidation of solutions from higher density grids into these actuation topologies.

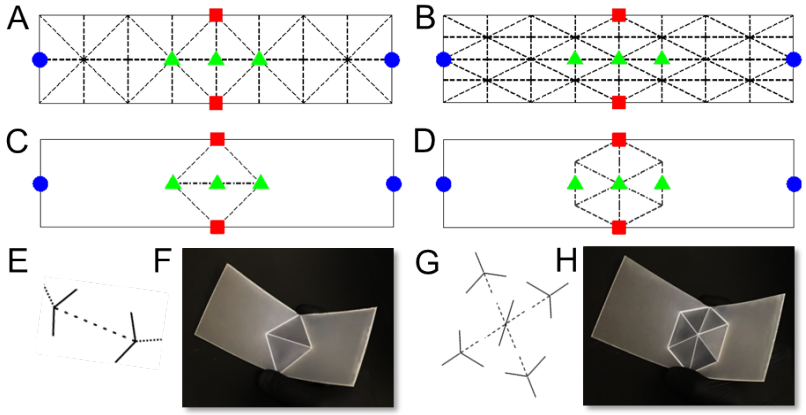

Figure 2: Building Block Actuating Units Based on Coupled-spherical Four-bar Mechanism

The actuator design problem of Figure 1B was solved on a set of increasingly refined reference grids. In order to find the least complex folding structure with the best performance, a constraint on the number of fold lines allowed in the final solution was applied. This is similar to an area or volume constraint applied in pixel-based topology optimization techniques [3]. The coarsest grid was a 4 by 1 array of the reference unit in the x and y directions, respectively (Figure 2A). The total number of fold lines within this grid was 38. Upon optimization with an

allowable fold line constraint of $l_0 = 0.2$, the 5 fold line pattern shown in Figure 2C was predicted. This particular structure is known within the compliant mechanism community as a coupled spherical four-bar mechanism and has been connected to a design in the action origami community known as the chomper [4,5]. A polypropylene (PP) model for the design was laser machined as shown in Figure 2F, and confirms that the coupled spherical 4-bar pattern successfully generates the desired actuation displacement. The mesh was then refined along the y direction using a 4 by 2 array of the grid unit within the original grid area (see Figure 2B). The number of fold lines within this new grid was 84, which was a 2.3x increase in design freedom from the coarse grid. However the connectivity of the mesh is altered by this refinement, meaning there is a set of designs that are mutually exclusive between both grids. For instance, the closed chomper solution in Figure 2C (closed meaning that bars of the mechanism form an interconnected loop) is not available in the refined mesh. The optimal solution on the refined mesh is instead a hexagonal actuating structure shown in Figure 2D and demonstrated in Figure 2H. On closer inspection, the fold pattern of the hexagonal unit consists of four coupled spherical 4-bar actuators tied together through a 6-bar node (see Figure 2G). However, the actuation of the hexagonal mechanism has a fundamental difference with the chomper mechanism, as folding occurs along center vertical axis of the grid in addition to folding along the outer edge of the mechanism. A comparison between the chomper and hexagonal mechanism will be renewed in a later section with the nodal location optimization.

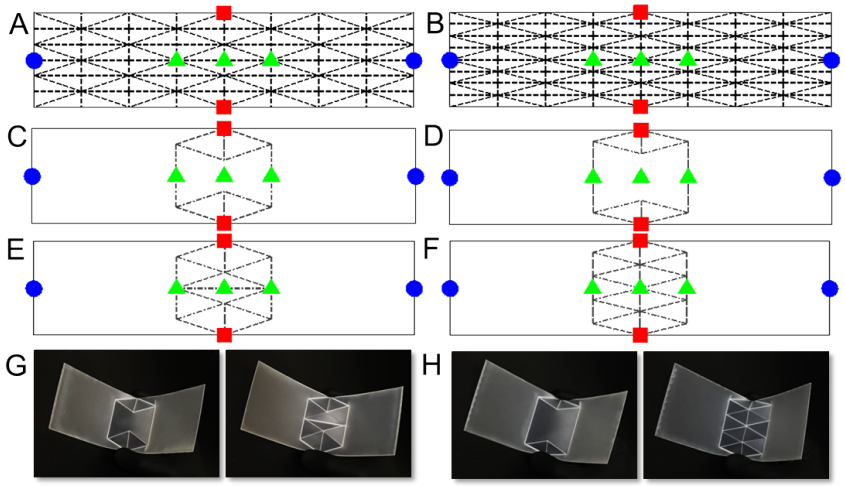

Figure 3: Variations of Actuating Building Block Units

Additional refinements of the reference grid were performed, including a 4 by 3 array with 130 fold lines (Figure 3A) and a 4 by 4 array with 176 fold lines (Figure 3B). Again, the increase in design freedom due to refinement comes with the trade-off of altered connectivity. The additional design freedom also reduces the effectiveness of the allowable fold line constraint to isolate the fundamental actuating units, as more intermediate solutions exist. In light of this effect, two solutions with slightly different allowable fold line constraints for each grid were presented. The simplest actuating fold structure that is shared between the 4 by 3 and 4 by 4 grids is shown in Figure 3C-D and were predicted with a constraint of $l_0 = 0.175$ and $l_0 = 0.2$, respectively. This solution resembles a hexagonal mechanism that has been separated and possesses the same key folding axes of the hexagonal mechanism (edge and vertical – see Figure 3G-H). With relaxation of the fold line constraint, unique solutions to each grid are predicted

(Figure 3E-F). The fold pattern on the 4 by 3 grid has the appearance of the separated hexagonal mechanism of Figure 3C with a chomper pattern inserted in the center. The 4 by 4 grid solution resembles two hexagonal mechanisms in series. Both structures reflect the odd/even nature of the grid refinement and suggest that the chomper and hexagonal mechanisms of Figure 2 are the key building blocks for actuation.

The mesh refinement strategy identified two basic building blocks of actuation, namely the chomper and the hexagonal actuator. Optimization on higher density grids predicted topologies that appeared to be variants of these two units. However, the presence of these variations highlights the dependency of the optimal solution on the choice of reference grid. Mesh refinement expands the design space, but does not retain the entire design space of coarser grids. A follow-up optimization was performed on the solutions from the fixed grid analysis to better understand this grid dependency. In the following case studies, the positions of interior nodes associated with fold lines, as predicted from the mesh refinement optimization, were optimally repositioned to improve the objective function. This analysis refines the active regions of the mesh and can inform how the original reference grid may have affected the solution.

3.4 Nodal Connectivity Optimization

Following the fold stiffness optimization, the positions of some selected nodes associated with the fold lines predicted from the previous optimizations were rearranged to further improve the design objective. Node position optimization of a reference grid topology has been employed in other mechanism design methods [6]. The number of fold lines is predetermined in this second optimization step, but their length and relative orientations toward each other are adjusted. In brief the nodal coordinates of the selected nodes are optimized by finding shifts from their original locations. The optimization problem associated with this phase of the design process is written as follows:

Find $\Delta x_1, \Delta x_2, \cdots, \Delta x_m, \Delta y_1, \Delta y_2, \cdots, \Delta y_n$ that

Maximize $f = \boldsymbol{c}^T \boldsymbol{u}$ (output deflection)

Subject to $\Delta x_k^{min} \leq \Delta x_k \leq \Delta x_k^{max} \; \forall \; k = 1,2,\cdots,m$

$\Delta y_k^{min} \leq \Delta y_k \leq \Delta y_k^{max} \; \forall \; k = 1,2,\cdots,n$

where Δx_k and Δy_k indicate the nodal coordinate shifts of the k[th] special node along the x- and y-directions; m and n are the number of nodes subject to the x- and y-shifts, respectively. The amount of shift is bounded by minimum and maximum values, ensuring that the connectivity of the underlying structure remains unchanged. The above optimization is solved using MATLAB's fmincon using the sequential quadratic programming (SQP) with estimated gradients calculated internally within the routine using the finite difference scheme. The presented design method, consisting of topology and shape optimization problems, is inspired by methods used for compliant mechanism designs by Hetrick and Kota [6].

Nodal location optimization was first applied to the coupled spherical four-bar mechanism (chomper) predicted on the coarse reference grid. Using the symmetry of the problem and the solution topology, only the x displacements of the active nodes on the center horizontal axis were allowed to move (see blue arrows Figure 4A). The displacements were constrained to remain in between their nearest neighbors, which prevented crossover

connectivity issues. The analysis predicted that the optimal chomper should have a shorter coupling distance between the two four-bar mechanisms. By shortening this coupling distance, the displacement performance increased 36% over the initial chomper design (Figure 4D). The altered reference grid that encompasses this solution is shown in Figure 4B. As a check, this new grid was input into the fold stiffness optimization routine and the same chomper mechanism was predicted. It is anticipated that an optimal ratio between the coupling distance of the 4-bar nodes and the moment arm of the applied loads exists. Confirmation of this optimal ratio could likely be independently verified using an analytical representation of the chomper mechanism.

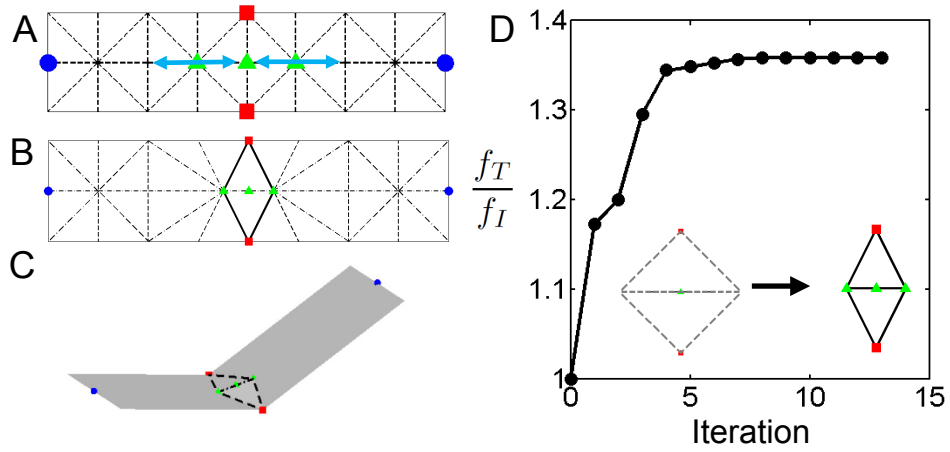

Figure 4: Optimization of Actuation Moment Arm of a Four-bar Mechanism

In the 4 by 2 refined grid, a hexagonal mechanism was predicted as an optimal actuator. However, the chomper solution was not available on this grid. In the next analysis, the nodes of the hexagonal mechanism were given the necessary freedom to recapture the chomper topology and in essence test whether the hexagonal actuator is a unique actuating unit or simply a substitute in the absence of a chomper solution. The active nodes of the hexagonal actuator were given x and y displacement freedom in accordance with the problem symmetry as indicated in Figure 5A. The nodal optimization did two unique adjustments: 1) the center line along the x axis was shortened, similar to the chomper optimization of Figure 4, and 2) the triangles centered along the x-axis contracted to a non-zero value. The consequence of these two adjustments can be seen in the updated mesh of Figure 5B and the deformed configuration of Figure 5C. The modified hexagonal actuator had a 26% performance gain over the original hexagonal solution (Figure 5D). The closure of the triangle along the x axis, which we define as pivot angle θ, was suggestive that the solution was attempting to become a chomper mechanism. However, performance of the hexagonal actuator is slightly better (~4%) than the chomper as seen in the plot of normalized displacement objective versus pivot angle of Figure 5E. The slight performance gain is likely due to the additional folding of the vertical fold axis in the hexagonal grid, which the non-zero pivot angle enables. The modified hexagonal solution was consistently predicted even under asymmetric perturbations of the initial hexagonal topology and was also predicted after repeating the fold stiffness optimization on the new grid in Figure 5B. Together, these results support the conclusion that the hexagonal and the chomper mechanisms are two unique building block topologies for fold-based actuation.

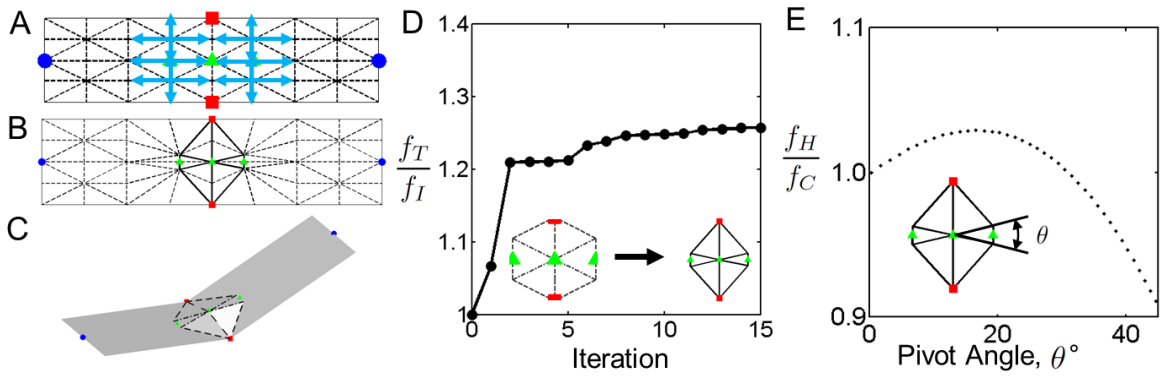

Figure 5: Optimization of Actuation Moment Arm of a Six-bar Mechanism

3.5 Optimal Networking of Actuators

In order to demonstrate the design process of mechanisms based on coupling of multiple origami actuating units, three more design problems are solved, using the chomper design as the basic actuating unit. This is done by applying the boundary conditions that represent the chomper design: two fixed nodes along a line and two downward input forces on either side of the line. Except for the first actuating unit, fixed nodes are switched to sliding nodes when inserting multiple actuating units to avoid over constraining the system. All the actuating units are inserted in pre-determined locations within a reference grid. The notation for the boundary conditions are the same as in the preceding section, except for the addition of xy −plane sliding nodes denoted with cyan squares.

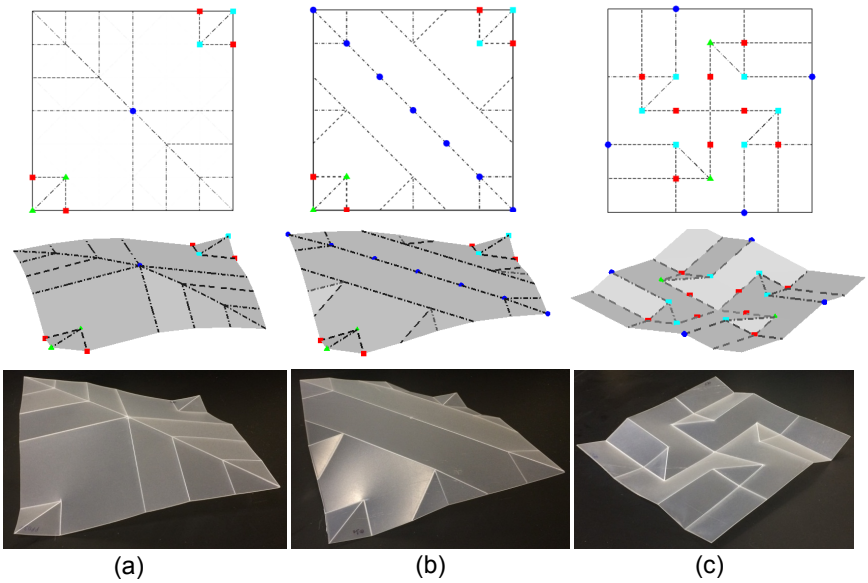

Figure 6: Optimized Fold Line Connectivity for Networked Actuation

In the first case study, chomper actuators are placed in opposing corners of a square reference grid. The objective is to maximize the out-of-plane motion of the center node of the reference grid (blue dot in Figure 6(a)). An intuitive solution for this design problem is to create a single fold along the diagonal from the upper left to lower right corner of the reference grid. In fact, the optimizer predicts this solution with a sufficiently tight fold line constraints (l_0 = 0.2,

f = -0.25). However, with a looser fold line constraint (l_0 = 0.375 – 0.475) the optimum solution achieves 60% better performance than the intuitive design (f = -0.4 vs f = -0.25). The optimum fold pattern includes the intuitive diagonal fold, but adds interior fold lines that soften the structure. These fold lines increase the objective performance by enabling the center of the grid to dome-up (Figure 6(a)). More complex designs ($l_0 \geq 0.5$) generated marginal performance gains (f = -0.40 vs $f \approx$ -0.41), indicating that the solution in Figure 6(a) was the best balance between performance and design complexity. Although not considered in the design problem, the optimum solution is a flat-foldable pattern if some of the fold directions are inverted (see Figure 7). In this specific case, the prediction of the optimization tool, combined with human insight, led to a design that would have otherwise been challenging to find.

The second case study consists of the same boundary conditions of the first case, but the objective function includes all of the nodes along the diagonal (Figure 6(b)). The optimum solution includes the intuitive diagonal fold line, but specifies an additional two fold lines parallel to the diagonal, along with relief folds at the mid-points of each edge of the grid. The additional fold lines increase the opening angle of the actuated arm, resulting in a slight performance gain. The decision to include these additional lines occurs late in the optimization process, indicating that they are not the dominant performance contributors (iteration 34 out of 43, f_{34}/f_{43} = 0.94). The performance improvement between the optimized solution and the intuitive diagonal fold line was 16% ($\underline{f}$ = -0.25 vs $\underline{f}$ = -0.29, normalized by the number of output nodes). Although modest in comparison to the first case study, performance improvements in this range may be sufficient for certain applications.

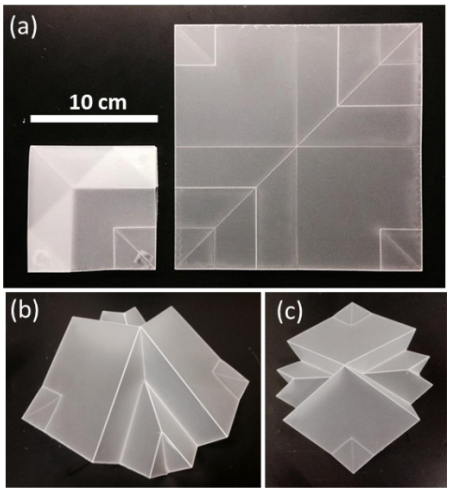

Figure 7: Flat Foldable Variation of the Optimal Solution in Figure 6

Lastly, the connectivity of a grid of four actuators with rotated orientations is optimized (Figure 6(c)). The objective is to maximize the out-of-plane displacement of four edge nodes, each of which is aligned with the hinge axis of an internally positioned actuator. Apart from knowing that the actuating axis will be a fold line, intuition on the location of other fold lines was limited. A rotational symmetry was imposed, given the nature of the boundary conditions, which reduced the number of design variables from 96 to 33. The per node displacement performance was $\underline{f}$ = -0.207 (l_0 = 0.4), which would be sufficient for this pattern to rest only on the objective nodes when actuated (inverted view of Figure 6(c)). This pattern was conserved over a modest range of fold line constraints (l_0 = 0.4 – 0.55), suggesting a relatively large local

minimum in the objective function. The additional fold lines in less constrained solutions again generated only marginal performance gains (l_0 = 0.575 – 0.95, f = -0.208), suggesting the plateauing of the performance at a tighter constraint at l_0 = 0.4.

3.6 Effect of Foldline Constraint on Solutions

Origami actuator design problems possess inherent symmetries associated with the grid, mechanical boundary conditions and the objective function. For instance in the design problems of Figures 1 through 3, a 180° degree rotation symmetry and both vertical and horizontal reflection symmetries are present. Problem symmetries are often exploited to reduce the design space and hence computational cost of optimization. However, enforcing symmetry eliminates the prediction of potentially better performing asymmetric designs. In addition, the discrete nature of fold line optimization (a.k.a. Is there a fold line present or not?) biases the design space to include asymmetric designs, as the fold line constraint and stiffness threshold can inhibit a symmetric distribution of folds. To better understand this effect, design problems with different symmetries were optimized over the entire range of the fold line constraint (l_0 = 0, no folds allowed, l_0 = 1 all folds allowed). The actuator design problem of the preceding sections was modified to only include vertical reflection point symmetry at the center of the grid, by shifting the applied loads along the horizontal axis (Figure 8A). No solutions are possible at very tight fold line constraints (l_0 < 0.15, Figure 8B), confirming the intuitive conclusion that a finite number of fold lines are necessary to achieve non-zero performance. The first fold pattern with non-zero performance is denoted by I_0, which includes the same symmetry of the design problem. The green circles in Figure 8B represent the fraction of fold lines used in the optimized design compared to the allowed number. Two distinct bands of solutions appear with increased allowable fold lines and are denoted by I and II in the Figure 8B. The topologies of band I and II also possess the symmetry of the initial design in Figure 8C. However, asymmetric solutions exist between these bands. The transition between symmetric and asymmetric solutions shown in this study highlights how the discrete nature of origami fold optimization, coupled with the fold line constraint, regulates the feasible design space. In addition, this study underscores how enforced symmetry eliminates interesting and potentially better performing asymmetric solutions. The benefits of increased computational savings through enforced symmetry must be weighed against the cost of missing better performing solutions.

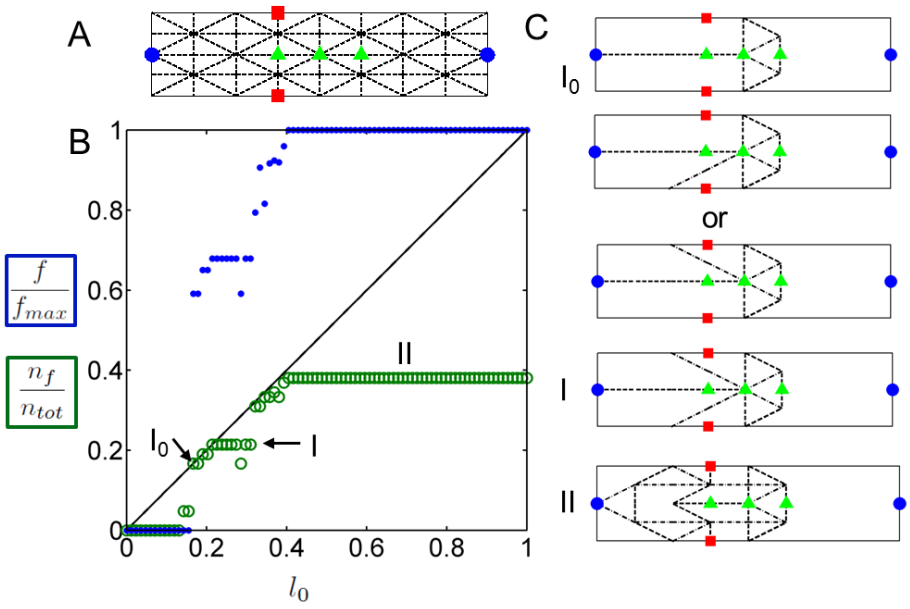

Figure 8: Optimal Mechanism Topologies across Foldlines Constraint

3.7 Challenges for Large Folding Design

The computational speed and simplicity of linear analysis comes with some limitations on the utility of the method as discussed earlier. A representative problem is solved using a preliminary implementation of nonlinear analysis using load increments and updated linear stiffness matrix to demonstrate when a design that is predicted by linear analysis may have non-optimal performance. Although this nonlinear implementation provides information as to when the design process requires nonlinear analysis, it does not accurately capture the stored strain energy along fold lines and requires many increments to follow the nonlinear load-displacement path. Derivation of the accurate increments and corrections terms is unlike those of conventional truss or beam-based formulations because of the introduction of fold stiffness.

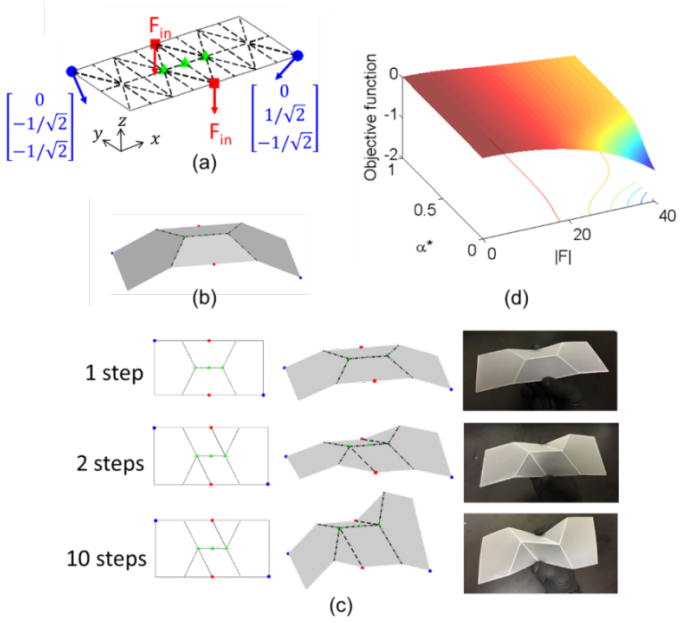

Figure 9: Comparison of Solutions Obtained Using Linear and Nonlinear Analyses

Figure 9(a) shows the problem specification with BCs and applied force similar to the chomper problem. The target output nodes are located at the upper left and lower right corners. The goal is to achieve a twist motion that creates deflection of the specified nodes in both y- and z-directions. This problem is solved using sequential quadratic programming (SQP) in Matlab's fmincon, which approximates the gradients using a finite-different scheme internally when the analytical gradients are not available. The optimal solution obtained using the linear analysis is shown in Figure 9(b), where only the z-displacement is achieved. The optimal solutions using multiple load steps are shown in Figure 9(c), along with the prototypes. The deformation achieves a twist motion with a combination of y- and z −displacements by adding foldlines from the ends of the centerline and the applied force locations. The deviation of the solutions using linear and nonlinear analyses can be illustrated by a surface plot of the objective function over the load $|\boldsymbol{F}|$ and design variable α^* corresponding to the fold stiffness of the additional foldlines (Figure 9(d)). The curve obtained as the cross section at $\alpha^* = 1$ corresponds to the evolution of the objective function over the load steps for the design in Figure 9(b). The slope is similar throughout the evolution, as the deflection mostly comes from the z-displacement. In contrast, the objective evolution corresponding to the twist design shown at the bottom of Figure 9(c) at $\alpha^* = 0$ exhibits a rapid change in the slope toward the end of the evolution, where the contribution of the y-displacement becomes significant and twist is more pronounced. This observation indicates that the optimization algorithm differentiates an origami design that involves a sequence of motions: 1) target nodes moving downward; 2) twisting, from that of a uniform motion. When the chomper problem is solved using multiple load steps, the solution obtained with linear analysis reappeared. This is consistent with the observation in the twist design, as the chomper does not involve sequenced motions.

In summary, linear analysis only captures the first phase of the motion and is insufficient when origami folding goes through sequences of fold motions. This is reminiscent of a finding reported in structural topology optimization involving large deformation in [7], where the nonlinear analysis predicts different solutions from those using linear analysis when deformations involve different phases of motion such as buckling or snap-through. In order to incorporate these types of mechanical phenomena into the design tool library, iterative techniques, such as the Newton Raphson method, need to be derived and implemented for the modified FEs used to simulate folding. In the following section, the Newton Raphson method was implemented for the truss element to model the snap-thru bifurcation of the "waterbomb" fold pattern. However, this implementation was simply used to analyze the structure, and additional work is needed to derive the sensitivities in order to use this nonlinear analysis within an optimization scheme. The first aim of the follow-on proposal for the origami effort is to develop this nonlinear mechanical analysis capability for large folding optimization.

3.8 Origami Pattern with a Tunable Dynamic Material Response

Action origami is an important subset of origami that includes designs that can actuate between two or more states. The prospect of robust, tunable actuators that are also inexpensive to manufacture motivates the identification and analysis of action origami structures. One such structure is the fundamental building block of the waterbomb origami pattern, which undergoes a snap-through bifurcation when mechanically loaded through a geometric instability. The snap-through structures has two stable states (Figure 10A,B) between which it dynamically transitions (<0.5s) when compressed beyond a critical load. Through a nonlinear implementation of the truss model, the critical load was determined to be tunable through modulating the fold stiffness (Figure 10C). Experimental results with laser machined polypropylene qualitatively agreed with

model predictions, but revealed a distinct difference in peak load between samples with and without the vertex (Figure 10D). Samples with the vertex intact required a small (~10%) increase in load to snap to the other stable state. This is due to the inversion of the folds near the vertex, while away from the vertex all the mountain and valley folds retain their orientation. The dynamic response of the snap-through structure shows potential for trigger, sensor, and toggle switch applications.

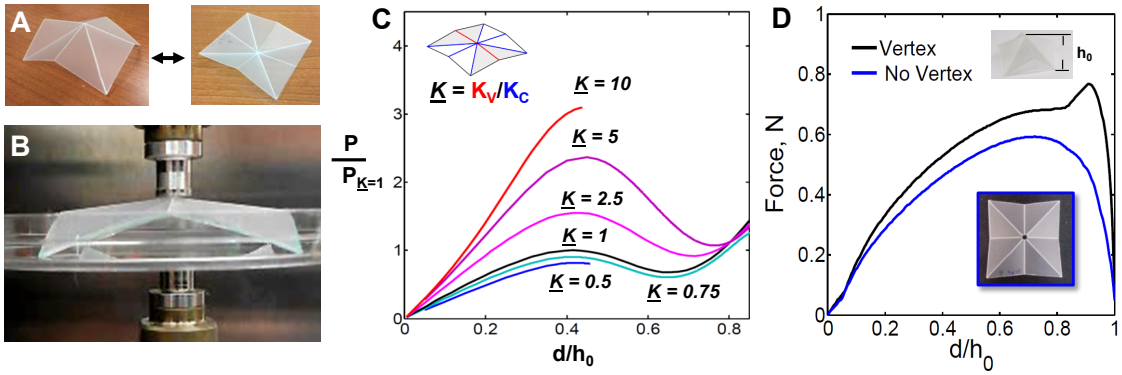

Figure 10: Tuning of Dynamic Snap-through Origami Structure via Fold Stiffness

The traditional paradigm for fatigue life prediction modeling applied to engine rotors is summarized in Figure 1. So-called crack initiation analysis is based on strain-life or stress-life methods and is often calibrated by total fatigue life results on small cylindrical specimens. The end of the crack initiation life phase is commonly assumed to correspond to the formation of an 0.030-inch surface crack. In order to account for normal material scatter, lower bound design curves (perhaps corresponding to 0.001 failure rates) are constructed through statistical analysis of the available smooth specimen data.

4. Frame Elements for Enhanced Mechanical Detail

Frame elements (*full beams*) are similar to truss elements, but allow for transverse loading and torsion. Additional DOFs, slopes and angle of twist, are assigned to each end of the frame element, along with the corresponding moments and torque *(12 DOFs per element)*. An analog of the torsion angle is used to explicitly define fold angle. With the additional DOFs, the in-plane and out-of-plane bending compliance may be locally optimized, enabling design of structures with facet and fold stiffness on similar orders of magnitude. By appropriately scaling the material moduli related to these modes of deformation, the response of the system can be separated out according to different strain energy levels. For instance, an origami structure with compliant, but inextensible facets can be defined using modest moments of inertia for the member while retaining a high axial stiffness (see Figure 11A). Similarly, folding-only deformations may be isolated by assigning the fold stiffness to be much smaller than the stiffness of stretching and bending, as shown in Figure 11B. The fold stiffness of the two dashed lines is varied relative to the fixed stiffness of the solid lines, highlighting how specific types of mode shapes can be energetically arranged through the redistribution of fold stiffness. Material properties do not vary through the thickness of the structure, but may be approximated though higher level parameters, such as an angle dependent fold stiffness or other material nonlinearity.

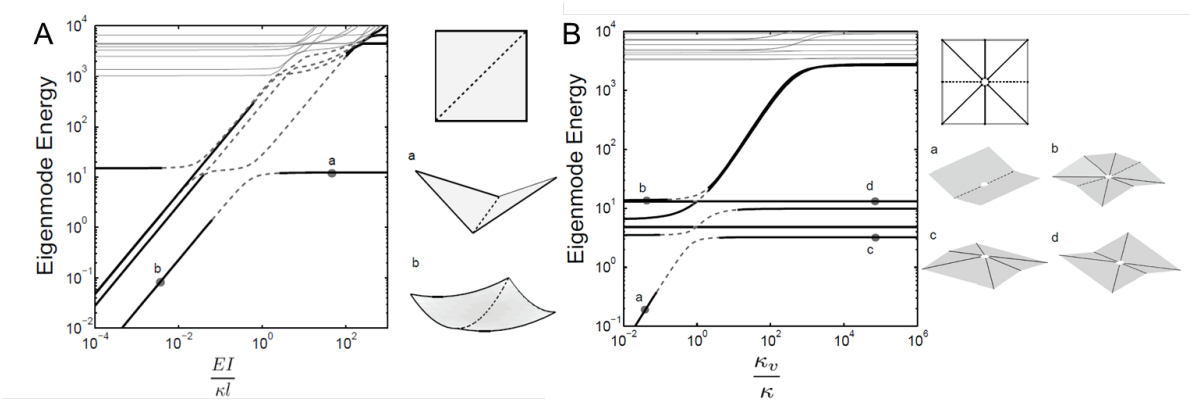

Figure 11: Energetic Ranking of Deformation Regimes in Frame-based Origami Model

4.1 Optimal Fold Directions for In-plane Compression

An in-house frame-based FE model was developed in order to specify the characteristics of the origami components: facets and foldlines explicitly, instead of the implicit characterization of folds used in the truss-based FE. The model was used in the design of an origami folding pattern for in-plane compression. Modal analysis was used to identify fold directions off of a flat configuration, by separating out higher-energy deformations such as stretching, bending and twisting across facets. The problem of finding how to fold a flat sheet using in-plane compression is cast as designing a perturbation off of the flat configuration by optimizing a linear combination of fold mode shapes.

The designed origami folds with a tight constraint on the perturbation energy input and a relaxed energy constraint are shown in Figure 12B and C, respectively. The more complex solution in Figure 12C required a two-fold increase in perturbation energy, but resulted in marginal performance improvement (< 2%) over the lower energy solution in Figure 12B. Perturbation energy is a particularly relevant metric for adaptive origami as the perturbation off of the flat configuration is the decider of the shape, which requires an orchestrated network of actuators or self-folding patterning. The origami design with a tighter energy constraint reduces

to the well-known Miura-ori pattern, which is empirically known for its efficiency in flat-folding to a compact structure. This feature motivates the use of the Miura-ori pattern as a replacement array for the warfighter's solar cell (Figure 12D-F). The Miura offers a five-fold increase in deployed area with a comparable carrying size to the current wallet type array. This is just one example of how origami design concepts can convert into engineering solutions supporting the AF mission.

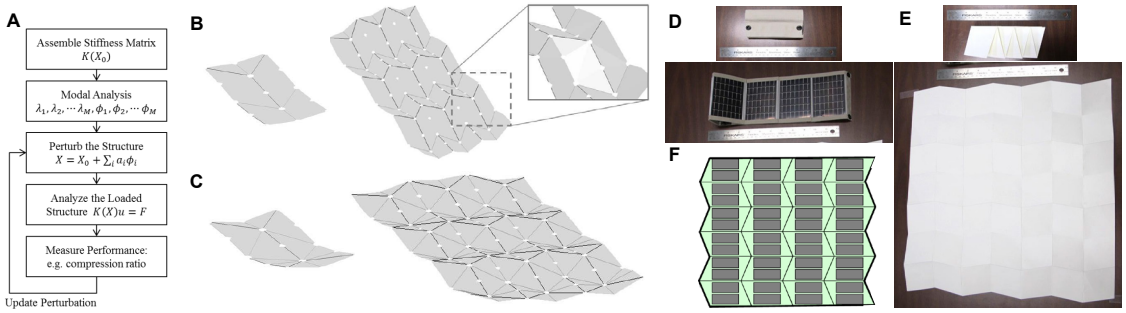

Figure 12: Optimization for In-plane Compression Converges to Miura-ori Pattern

5. Material Failure Behavior Underlying Fold Performance

5.1 Identified Terminology to Distinguish Types of Folding

Origami terminology of fold, bend, and crease are currently poorly defined terms and are often used interchangeably by artists. A need therefore exists for scientists and engineers to develop rigid definitions and establish distinguishing characteristics of these terms to create a universal language for the engineering community. Here, it is proposed that the term fold be used as a broad term comprised of the subcategories bend and crease. A bend refers to elastic, non-localized, recoverable deformation and is represented on a force-deformation curve in Figure 13A as the darker region at low deformations. Formation of a crease begins when a specimen is bent passed the onset of plastic deformation resulting in localized and some degree of non-recoverable deformation shown as the lighter region in Figure 13A.

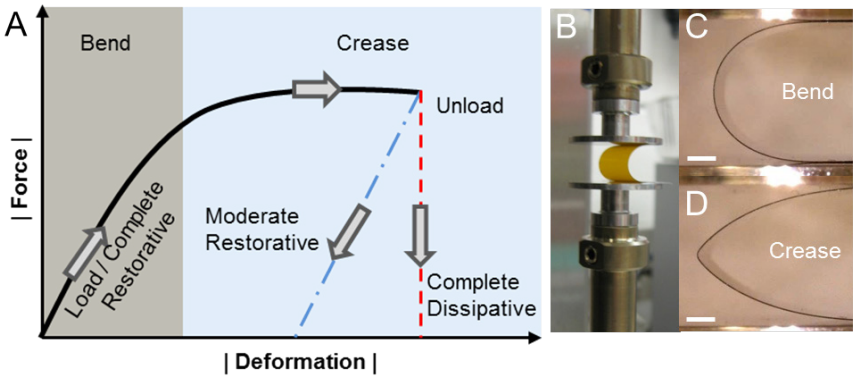

Figure 13: Fold Behavior Defined According to Loading Regime

5.2 Custom Fold Test and Characterized Failure Morphology

Crease behavior ultimately depends on the failure mechanism and dissipative nature of the material. However, this is an underdeveloped area of research for polymeric materials. Most fold research focuses on paper and paperboard for the packaging industry where it is critical to generate reproducible creases with predictable bending properties for automated assembly. A number of testing methods exist to measure bending stiffness, but are generally limited to small fold angles and low strain regime, and do not evaluate crease formation. Therefore, a new folding technique was developed to overcome these limitations. Polymer films were bent to fit between parallel compression plates (Figure 13B) of a displacement controlled mechanical testing apparatus equipped with a high precision force transducer. Specimens were loaded at a rate of 10 mm/min until the gap distance reached twice the specimen thickness, loading through the bend (Figure 13C) and crease (Figure 13D) regimes. Energy dissipation due to creasing was characterized by comparing the areas under the loading and unloading force-displacement curves. The crease surface morphology was evaluated using polarized microscopy, scanning electron microscopy (SEM), and profilometry (Figure 14 A-C). Identification of the crease birefringence with the polarized microscope enabled approximate measurement of the crease width. Figure 14B shows an example of interior crease surface (compression) deformation for Kapton manifested as localized buckling. The periodicity of the surface wrinkling correlates with profilometry width measurement, with height measurements indicating deformation intensity. SEM micrographs provide an additional estimate of the crease surface morphology,

collectively showing that increased localized plastic deformation drives increases in residual fold angle retention.

5.3 Prediction of Residual Fold Angle

The fold test facilitates direct measurement of residual fold angle, fold stiffness, and morphological details of the material failure at the crease. However, for specific applications where fold angle is of singular interest, a model of a crease deformation may be able computationally predict versus empirically determine fold angle performance. Using readily available uniaxial tension data, the polymer films near the crease were modeled as beam under pure bending. Assuming a linear strain field through the thickness of the beam, the strain field was calculated based on the applied curvature. Elastic and plastic strains were identified in the beam cross-section using the yield point from experimental uniaxial tension stress-strain curves. Unavailable compression stress-strain curves were taken to be symmetric to the tension data. After computationally accruing plastic deformation by applying curvature to the beam, residual curvature is calculated by solving zero moment balance across the beam cross-section. Residual fold angle is then calculated from the residual curvature and an estimation of the plastic zone of the beam, currently taken as the experimental cease width. The residual fold angle contour plot shown in Figure 14E shows the dependence of residual fold angle on applied curvature and specimen thickness, using uniaxial tension data for Kapton. Experimental fold angles for Kapton (dots) overlay the model data in Figure 14E and demonstrate good agreement, even without a fitting parameter. However, the model is not completely independent of the folding test data, as measured crease width was need to estimate the plastic zone. A database of crease width as function of applied curvature and thickness is being created to identify trends, which may eliminate the need to testing across all material and specimen geometries.

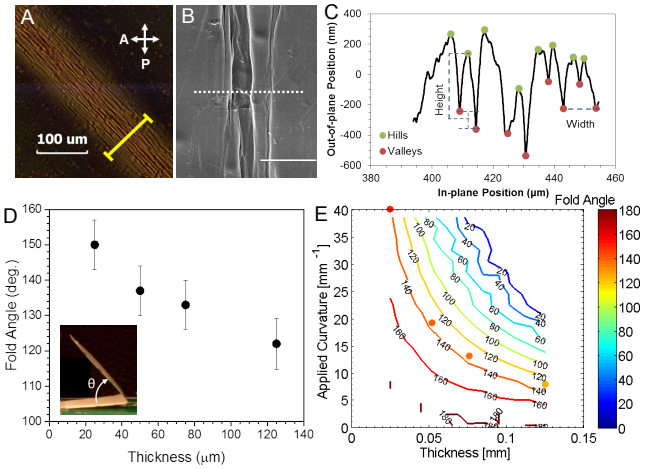

Figure 14: Prediction of Residual Fold Angle

6. Self-Folding Materials

6.1 Reprogrammable Shape Memory Nafion

Self-folding origami requires materials that generate strain or release stored strain in response to a stimulus. Shape memory polymers allow mechanically induced strains to be temporarily stored, and then released with heating above the storage temperature. Complex, folded shapes can be generated through this shape memory response. The temporary shape of Nafion was discovered to be reversibly locked through local patterning with a basic solution (NaOH). Base treatment deprotonates the side chain of the Nafion polymer increasing the stiffness and temperature cooperative relaxation (100 °C - T_{H^+} vs. 260 °C - T_{Na^+}) of the polymer (Figure 15A through C). By patterning the base locally, the film will take on complex 3D conformations when released due to the incompatibility of the strain fields between the locked and unlocked regions. The 2D to 3D transformation of a uniaxial stretched bar with a locked strip in the center was predicted by FE modeling (Figure 15D). The simulations showed that only a through-thickness penetration of the locking reagent, with increased locked area on bottom vs the top (+10% A_{bot} vs A_{top}) was capable of generating the upward bend of the film when thermally released (Figure 15E through I). Precise patterning of the locking agent was performed through printing, as seen with the honeycomb structure in Figure 15J through K. Inverse patterning is also possible, where by the entire film is locked in the stretched state and then select regions are unlocked with a localized treatment of an acidic solution, such as HCl. Inverse patterning is advantageous for origami applications because only the hinge will deform at the release temperature, while the facets remain locked (Figure 15L). The robust temperature separation of this chemical locking strategy, combined with the precision of the printing approach, make Nafion a novel candidate for single-use, deployable, origami structures.

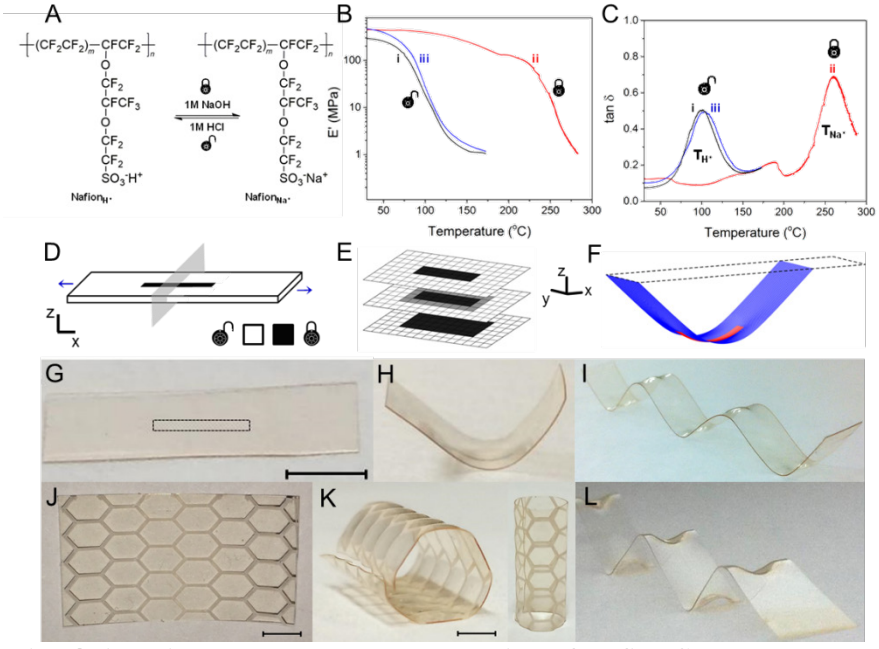

Figure 15: Origami through Temporary Locking of Nafion Shape Memory Effect

6.2 Reversible LCE Actuation

Many adaptive origami applications require cyclic actuation, such as opening and closing of a solar array or the precision tuning of an airfoil's topology for optimal lift. Such applications

necessitate stimuli response materials with the ability to precisely and reversibly actuate through a range of folding motions. LCEs in development at AFRL generate strains up to 60% and show good reversibility in preliminary testing (> 100 cycles). Using an in-house, optical patterning tool, the local director of the LCEs can be arbitrarily oriented in the plane of the film, as well as through-thickness for films under 100 μm thick. To facilitate the preparation of spatially heterogeneous LCEs, we assembled an optical patterning system in which the polarization of an irradiating 445-nm laser over an area as small as 0.01 mm^2 is controlled. The optical setup manipulates the local surface alignment of the LC cells and subsequently controls the mechanical response of the LCE. Together, the large strain generation and novel optical patterning capability of the director makes the LCE material system well-posed for a design optimization approach of the mechanical response.

The objective of the design problem is to match the deformed LCE film to a hinge shape through the optimization of strain distribution. The recent report on the preparation of spatially patterned LCEs illustrated a use of twisted nematic alignment to introduce localized folding [8]. The twisted nematic orientation is a self-organized functionally graded orientation that naturally generates a local strain gradient through the thickness of the material along the primary (x'-) direction. However, this deformation is volume conserving and as such is accompanied by strains in the orthogonal directions, leading to anti-clastic bending as discussed in [9,10]. In certain configurations, this curved fold can influence surrounding hinges to cause spontaneous misfolding. An optimization problem is formulated to design a patterned LCE film that conforms to an ideal hinge shape on heating. Although a large fold angle at a high temperature is desirable in order to extrapolate the origami geometry toward closure, more emphasis is placed on controlling the shape in this formulation.

The mechanical analysis for the design update is based upon an 8 node brick FE with linear elastic material behavior. The design domain consists of a 5- by 5-mm specimen discretized into a 50 by 50 mesh with an order parameter and director orientation assigned to each element. The model assumes 1) small displacement, 2) small strains (0.5%), 3) the spontaneous strain in disordered pixels is zero, and 4) the director orientation through the thickness changes linearly and can be adequately resolved by four brick layers. The linear analysis significantly reduces the computational cost of the optimization because the load step is not incremented and the stiffness matrix does not require updates. However, the small displacement assumption of the linear analysis focuses the optimization on finding the pattern needed to initiate folding and not necessarily the optimal solution for large folding.

Nonlinear mechanical analysis was employed to evaluate the folding performance of the predicted designs at larger strains (≥ 2.5%). The nonlinear analysis was performed in ANSYS 11.0 using four node shell elements with four layers. The director orientation profile from the optimal solution was assigned using the built-in element orientation angle ϕ, and was assigned for each element in a 50 by 50 mesh. The spontaneous strain of the LCE was assigned using the thermal expansion interface with anisotropic coefficients that were volume preserving. The shell element analysis accounted for geometric nonlinearity using an incremental thermal load step and an update of the stiffness matrix within a Newton Raphson iterative scheme. After the computational analysis in both the small and large strain regimes, the order and director orientation profiles of the design are output to the patterning system for fabrication and tested via uniform heating. The design and experimental feedback process discussed above is outline in the flowchart of Figure 16.

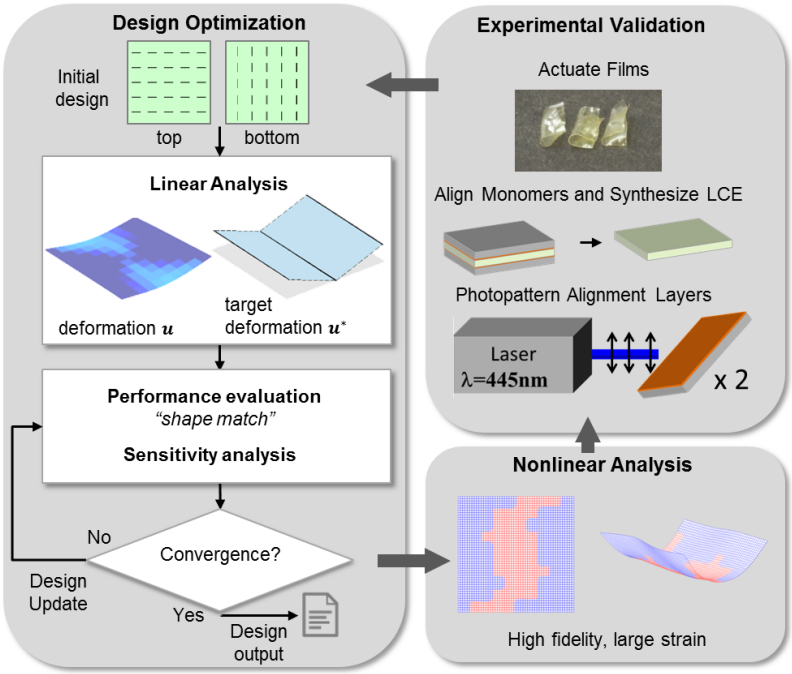

Figure 16: Schematic of the LCN Design and Fabrication Feedback Process

The optimal order/disorder pattern and director orientation distribution are shown in Figure 17C, along with those of the twist nematic hinges (Figure 17A and B). Comparison of the director orientation distributions reveals that the optimal design achieves folding through a similar mechanism as the twisted nematic hinges: contraction in the $\phi = 0°$ direction at the top and expansion in the $\phi = 90°$ direction at the bottom surface, to create a strain gradient through thickness. However, triangular distributions of active areas, instead of rectangular regions, are observed with slanted director orientations at the edges of triangular regions. These features somewhat resemble parts of a +1 topological defect. The top layer is a segmented +1 azimuthal disclination with continually rotating director orientations creating circular profiles with a singularity at the center; the bottom layer is a segmented +1 radial disclination. The orientation of the director rotates 90° through the thickness of the film from radial to azimuthal, creating a pattern called radimuthal presented in[10,11]. In the optimal hinge design, the distribution of inactive regions leads to a removal of saddling by reducing the strain near the center, and re-distribution of active regions towards the outer edges helps to evoke the desired, folding motion.

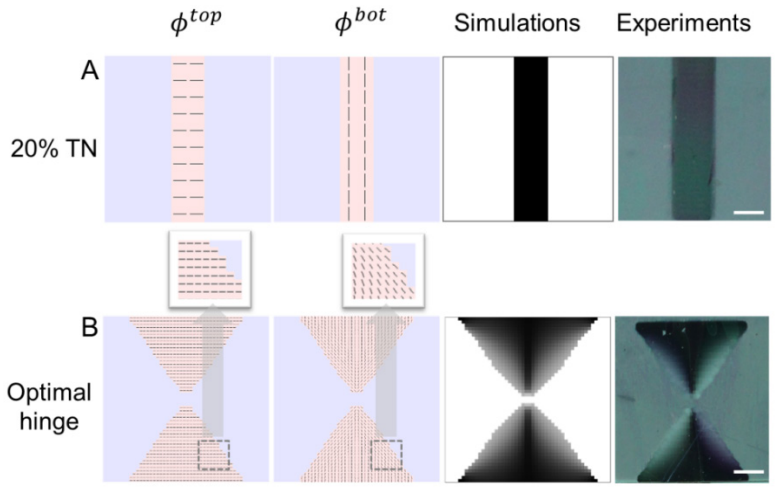

Figure 17: Optimal LCE Director Orientation Pattern for Origami Hinges

A box design inspired by the optimal hinge is shown in Figure 18D. Four smoothed optimal hinges are patterned at the base of each flap and networked through a rotation and superposition of the overlapped director profiles. The director orientation is rotated by 90° through thickness. Again, the design resembles a discrete approximation of a radimuthal pattern around each corner of the box base, but with a quarter of the pattern cut off. The image of the fabricated LCE film under a cross-polarizer is shown in Figure 18F. Upon heating the film undergoes a desired deformation with all four flaps folding up, creating a box (see Figure 18G).

The fabricated box pattern in Figure 18F exhibits multi-stability with deformation modes other than a box shape in nearby energy levels, which may be accessed by applying forces near hinges. Depending on the sample preparation and actuation conditions, the deformation may be steered into an undesirable mode. Potential contributing factors to this discrepancy include some level of order in un-patterned regions, the effect of domain interfaces, temperature distribution, elastodynamic effect and anisotropy of the constituent material. Although these issues are not addressed in our current model, use of the initial deformation in the design process was effective in alleviating the mechanical frustration of the hinge network and improved the likelihood of folding in the desired direction.

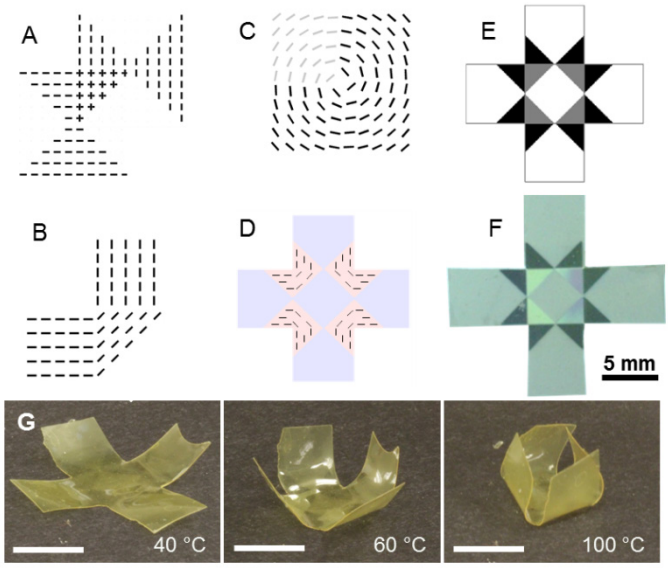

Figure 18: Multi-hinge Network Solution Inspired by the Optimal Hinge Design

6.3 Large Design Domain LCE Optimization

In addition to the box LCE design that was inspired by the single hinge solution, a design optimization problem for the box domain was investigated. This study tested the optimality of the composite single hinge network of Figure 18, while simultaneously evaluating the robustness of the optimization method in a large design space (300+). Previously used design variables: LCE director orientations at the top and bottom layers were defined in multiple sub-domains and optimized simultaneously to achieve a more complex target shape.

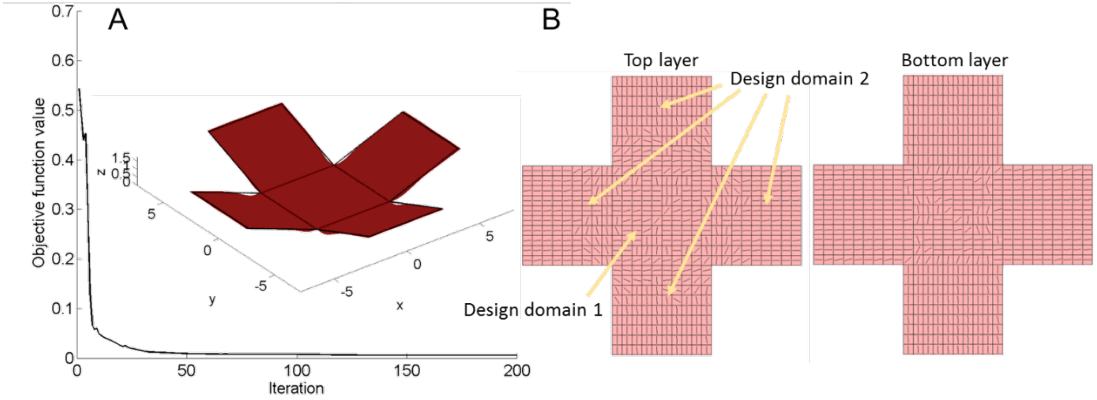

Figure 19: Large-scale LCE Design Optimization

Figure 19 shows an example of this design formulation. The sample film is assumed to be cut into a cross shape composed of five squares. The design goal is to actuate a network of four hinges to create a folding box. The four squares that are to be the flaps were assumed to share the same strain distribution based on the symmetry of the target shape, reducing the computational effort of the design process significantly. The entire domain was allowed to be active in this example. The iteration history of the objective function values and the deformed configuration of the optimal design (see Figure 18A) indicate a smooth convergence to a design that achieves a deformation that matches well with the target shape. However, the optimal design depicted in

Figure 19B indicates rapidly altering LCE director orientations, which posed a significant challenge in fabricating a sample that follows a predicted deformation upon actuation.

The results of this study highlighted some of the limitations of our current design formulation, which utilized many simplifications on the material modeling. One of our key material assumptions that proved to be too limiting, in the case of the above example, was that LCE domain interfaces along which director orientations change have negligible effects on the overall deformation. This assumption allowed for an optimal design with many interfaces. The large deviation between the predicted and observed sample behaviors indicates that the material model requires modifications for design problems with moderately complex target shapes (beyond a hinge). Alternatively, the design formulation may be modified to limit the number of LCE domain interfaces. These studies have shown to be valuable, not only for achieving specific design goals, but also for understanding the adequate level of accuracy in material modeling required in the context of design optimization. The lessons learned through these studies are not limited to patterned LCEs, but are applicable to other materials and material processing techniques that can offer tailored gradient or distribution of properties such as Young's modulus.

6.4 Additive Manufacturing Strategies for Local Thermal Actuation

Control of actuation can be introduced by localizing the thermal stimulus of the LCE. Localized joule heating via inkjet-printed Ag resistors has been experimentally demonstrated (Figure 20), which opens the door for real-time, sequenced folding. Device fabrication on a substrate that changes shape with temperature places a variety of demands on the method of fabrication, including low processing temperatures and strain resistance. A variety of printable conductive materials and printing techniques were studied. Among the studied conductive inks: colloidal based (nanoparticles) inks were successfully printed on the LCE material. However, the required sintering temperature and time to become conductive was not compatible with the LCE materials. Carbon-nanotube-based ink was successfully printed on LCE material as well, but its limited conductivity required the application of very high voltages to reach the desired temperature. A reactive Ag ink compatible with the LCE material was selected; this ink produces conductive printed features at room temperature and archives very high conductivity upon annealing at 100 °C for 15 minutes. Both inkjet and aerosol jet printing techniques were successfully utilized to print the conductive traces on LCE. The Aerosol jet printer was mainly used because of the much higher printing resolution.

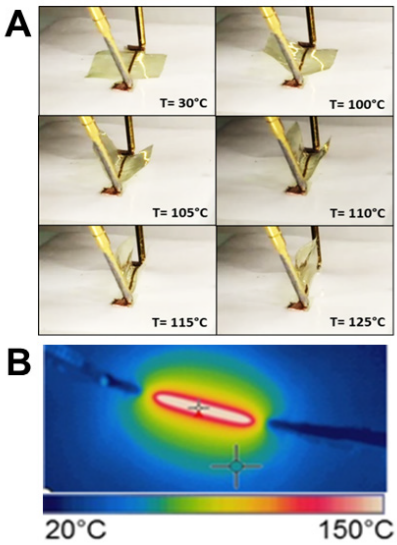

Figure 20: Local Thermal Actuation of LCE Hinge

(LCE hinge with printed Ag line. A) Hinge goes from flat state before heating to 180° fold after Joule heating (1V, 250 mA). B) IR image of the heated hinge demonstrating the intensity (150°C) and localization of this approach.)

Among the advantages of utilizing localized Joule heating is the ability to quickly and precisely control the temperature by adjusting the applied voltage. In Figure 20, single joule heated hinge is shown in the flat and folded states with various folding angles. The IR image of Figure 20B shows how Joule heating allows for localize heating with very precise temperature control and fast heating and cooling process. Utilizing multiple hinges is possible to create more complex structures, for instance 4 hinges organized in a square shape configuration were prepared and made actuate through localized heating to form an open box structure (Figure 21).

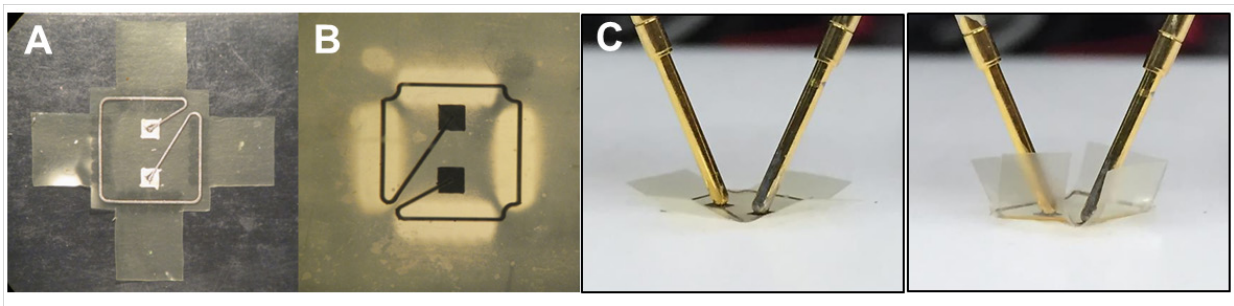

Figure 21: Large-scale LCE Design Domain

6.5 Homeotropic LCE Hinge

The optical LCE patterning used in the preceding sections can only program the in-plane orientation of the director on both the top and bottom surfaces of the film. With this technique, a twisted nematic liquid crystal pattern, where the orientation of the nematic director rotates by 90° through the sample thickness, was identified as a key design motif for folding. The twisted nematic motif is capable of generating fold radii of curvature on the order of five times the thickness. Sharper radii can be achieved by controlling the orientation of the LCE director along thickness direction, known as homeotropic alignment. Homeotropic alignment is the state in which a rod-like liquid crystalline molecule aligns perpendicularly to the substrate (Figure 22A). In order to get homeotropic orientation it is necessary to pretreat the surface either mechanically

or chemically. One of the chemical treatments available consists in treating the substrate with a special polyimide (PI 1211) [12].

Utilizing direct writing of the polyimide alignment layer by an aerosol jet printer, complex, high resolution patterns of homeotropic alignment layer were easily prepared on specific regions of the substrate. Figure 4.8B shows a polarized microscope image of a 500µm wide line of homeotropic aligned LCE between planar aligned LCE, a dark field is observed between crossed polarizers because homeotropic alignment is not optically anisotropic.

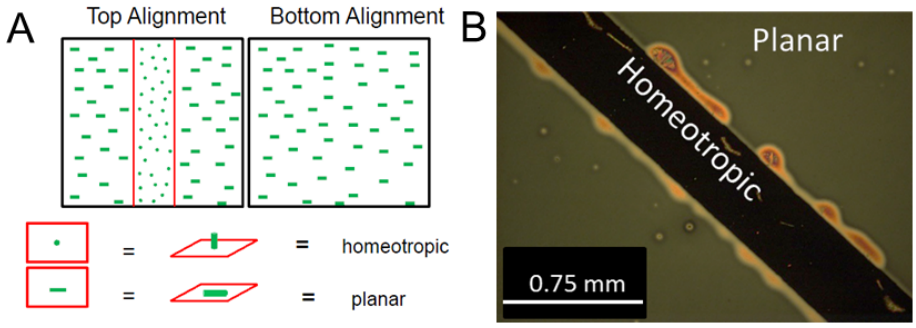

Figure 22: Homeotropic Patterning for Precise Fold Lines

Figure 23 shows the thermal response of the homeotropic LCE hinge. It's clear that the homeotropic hinge produce extremely sharp folding angle compare to the one obtained by the twisted nematic LCE hinge previously prepared. Because of a slightly different chemical composition the homeotropic LCE hinge required higher temperature to actuate (T~ 200 °C) compared to the previously prepared twisted nematic hinge (T~130 °C).

The higher temperature needed to actuate the homeotropic hinge in combination with the higher strains produced by this material caused failure of the printed conductive traces utilized for the localized Joule heating during the actuation process. To overcome this challenge a new stretchable conductive ink was used for this system. The Ag-TPU ink (2- to 4-µm Ag-flakes dispersed in thermoplastic polyurethanes) is a stretchable conductive ink currently under development at AFRL. This ink was shown to be compatible with the LCE material and to be able to withstand temperatures up to 230 °C. The use of the Ag-TPU conductive trace as a resistor for localized Joule heating of homeotropic LCE hinges is currently under investigation.

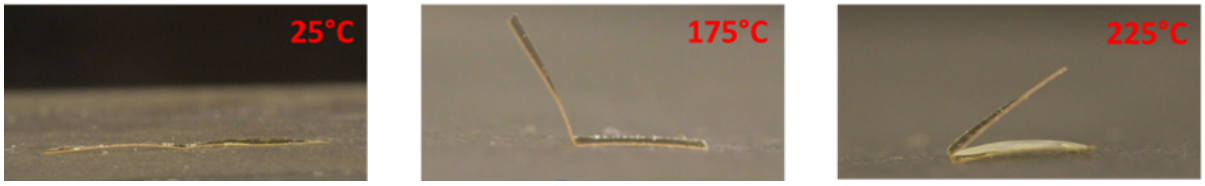

Figure 23: Folding of a Homeotropic LCE Hinge

7. Origami for Electromagnetic Tuning

Reconfigurable RF devices hold great promise as adaptive antennas, signal filters, reflectors, and ambient RF energy harvesters. Origami design techniques offer an efficient description of geometric reconfiguration through a series of folding operations. However, the effect of folding RF components on their EM performances is largely unknown. This motivated the investigation of relationships between folded geometries and EM performances of RF devices. As an example, resonance characteristics of FSSs were examined on periodic arrays composed of conducting traces printed on four origami tessellations.

7.1 Rigid Origami Simulation of Tessellations

Two basic units (Figure 24A) were combined to construct four origami tessellations (Figure 24B), which fold to shrink their projected area while keeping their overall curvature to zero. Folded configurations of each of these tessellations are computed using the rigid origami model that traces isometric mapping with no elastic deformations. Snapshots of the fold simulation of tessellations composed of 4 by 4 units of periodicity (4 by 5 units for inverted Miura-ori) are shown in Figure 24C.

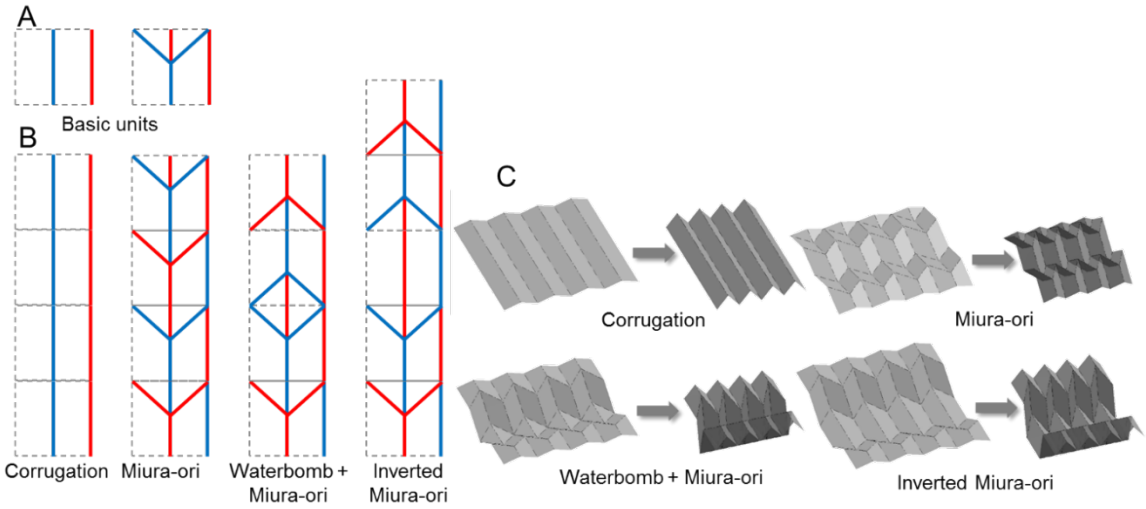

Figure 24: Origami Tessellations Used for FSS Simulations

7.2 Electromagnetic Analysis in COMSOL Multiphysics

Each square unit of the tessellation is decorated with either of two types of conducting traces: dipoles or square loop (Figure 25A). The geometric configuration of each FSS design is drawn in COMSOL RF module, and an FE analysis is carried out to evaluate their EM performances (see Figure 25B for the setup). Key assumptions for the EM simulation include: 1) substrate is a very thin dielectric ($\ll 0.01\lambda$) with negligible effects in the range of frequencies of interest, and 2) conducting prints are approximately lossless. These assumptions may be subject to modifications for higher fidelity analysis, but are adequate for the goal of this study, which is to understand the underlying principles of tuning phenomenon in folded EM components. The vector Helmholtz formulation of Maxwell's equations is solved to find the electric field distribution. The transmission coefficient S_{21} is computed using the electric field and its magnitude is plotted in a log scale (dB) over a range of frequencies to examine the resonant behavior of each design.

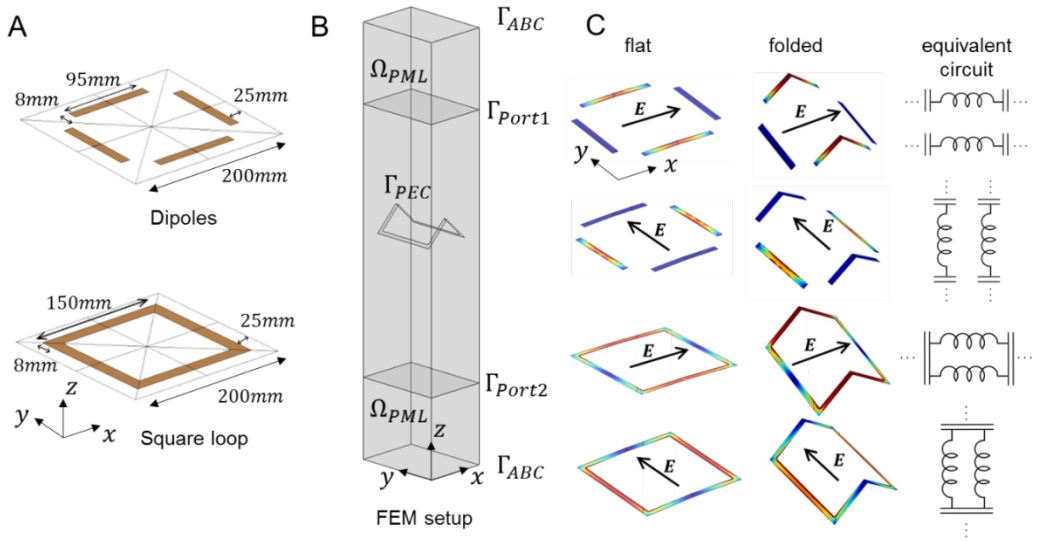

Figure 25: Electromagnetic Analysis Setup for Simulation of Folded FSS

The design in Figure 25 A has two sets of dipoles oriented along the x- and y-directions. When this pattern is excited with the electric field polarized along the x-direction, the two dipoles aligned in the x-direction exhibit a current flow at the resonant frequency, as shown in Figure 25C, top. An equivalent circuit at this polarization depicted in Figure 25C, right, is an LC (inductor-capacitor) circuit with an assumption of no resistive loss. A similar phenomenon is observed when the substrate is folded, creating folds in the excited dipoles. When the pattern is excited with a y-polarization, the other two dipoles experience a current flow, resulting in the same equivalent circuit aligned along the y-direction. Similar surface current plots are produced for the square loop design in Figure 25C, bottom. At resonance, the segments aligned with the electric field direction are excited as before. The equivalent circuit for square loops has two parallel inductors connected through the segments of the conductor orthogonal to the electric field direction.

7.3 Tessellation Patterns and Resonance Shift

The frequency at which FSSs exhibit stop- or pass-bands depends on many factors including the conductive trace geometry and the placement of the prints. The frequency sweeps of the transmission coefficients for a corrugated sheet with dipoles are plotted in Figure 26 at four different fold configurations indicated by time step t. The resonance is observed at 1.38GHz at the initial flat state (t=1) for both x- and y-polarizations, reflecting the design's four-fold rotational symmetry. However, the symmetry is broken once the pattern is folded, and different resonance characteristics are observed. The resonance shifts upward as the separation distance along the x-direction becomes smaller with folding, whose rate is higher when the dipoles along the y-directions are excited. When dipoles are printed on the Miura-ori, separation in both x- and y-directions become smaller as the substrate is folded, leading to a different resonance shift trend (Figure 27, left). Summaries of resonance shift trends are plotted for both x- and y-polarizations in Figure 28A and B, respectively.

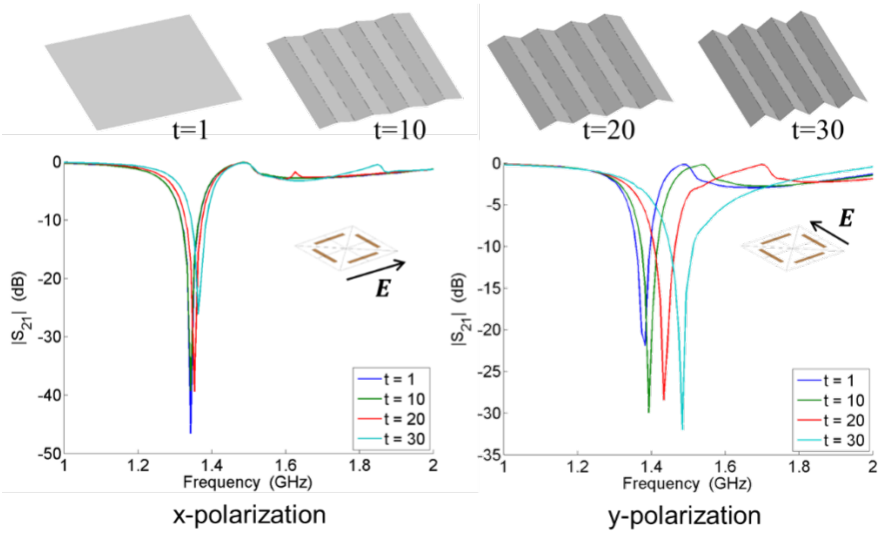

Figure 26: Transmission Coefficients for Dipoles Printed on a Corrugation

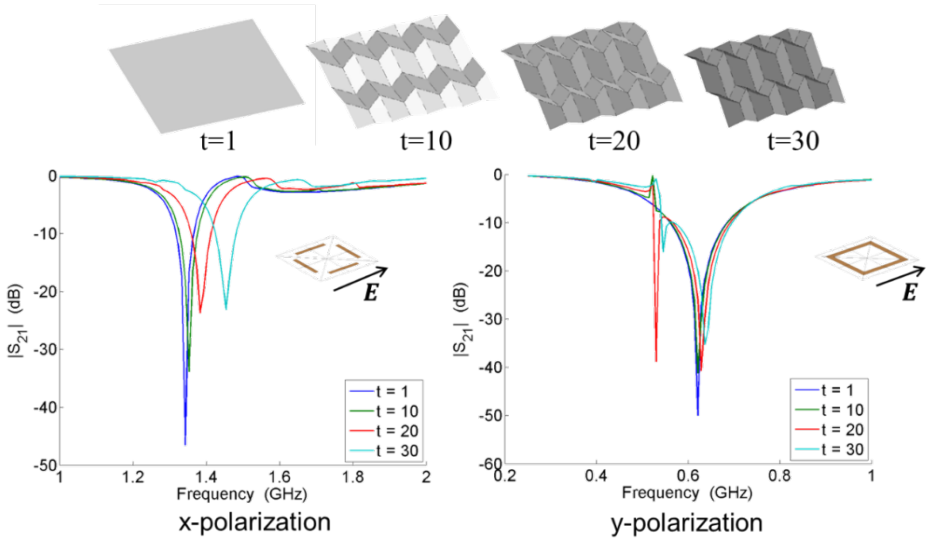

Figure 27: Transmission Coefficients for Dipoles and Square Loops on Miura-ori

As the sheet is folded, its x-projection becomes smaller; its y-projection also becomes smaller at different rates (0 in case of corrugation). In FSSs excited with x-polarization, the higher rate of the y-projection change coincides with the higher rate of the resonant frequency shift. This implies that the separation distance parallel to the excited dipoles has the dominant effect due to the alteration in the equivalent inductance. In FSSs excited with y-polarization, the rate of resonance shift is similar for all four patterns, supporting the previously stated conjecture. The slightly lower rate of resonance shift observed in the corrugation may be due to the bend along the dipoles created in all patterns but the corrugation.

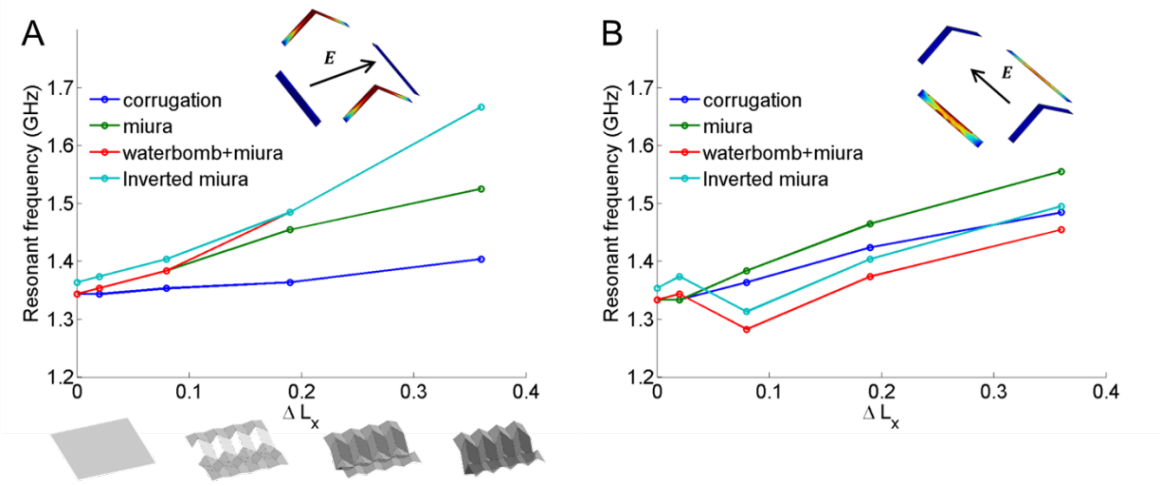

Figure 28: Resonances in Transmission Coefficients for Folded FSSs with Dipoles

Square loops printed on the Miura-ori exhibit a very small shift (2.4%) in resonance as seen in Figure 27, right. A consistent trend of having a small resonance shift is seen in the summary plots in Figure 29. A possible explanation for this is because the location of the resonance in loops is primarily determined by its perimeter, and coupling effects from the separation distance has a less significant effect on the resonance shift of the dominant frequency. However, in all patterns except for the corrugation, an extra resonance appears at a lower frequency towards large fold (see Figure 27B). As this is not observed in square loops printed on corrugation, nor in the fold configurations near the flat state, the effect is hypothesized to be a consequence of adjacent elements coupling along the y-separation distance (fixed in corrugated pattern) and deformation of the loops from planar to bent configurations. A series of numerical experiments were performed to isolate the coupling mechanism responsible for this lower frequency resonance (see Figure 30).

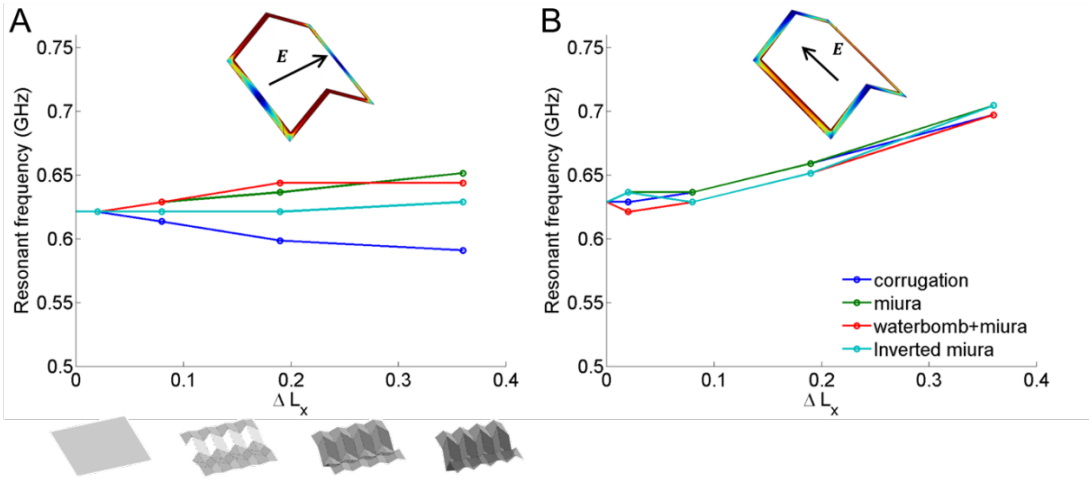

Figure 29: Resonances in Transmission Coefficients for Folded FSSs with Square Loops

As the substrate with square loop prints is folded in Miura-ori pattern, several geometric alterations to the conducting square loops occur: 1) the separation distance between the adjacent

loops becomes smaller; 2) the dihedral angle between the planes hosting the adjacent loops becomes smaller; 3) bends are introduced on the conductive trace. As shown in Figure 30A through C, none of the geometric changes, isolated as described above, reproduced the additional lower resonance. However, when two adjacent loops folded along Miura-ori are simulated as in Figure 30D, the lower resonance appeared. This indicates that the lower resonance is a result of creating bends on the loops and coupling of elements along the y-direction.

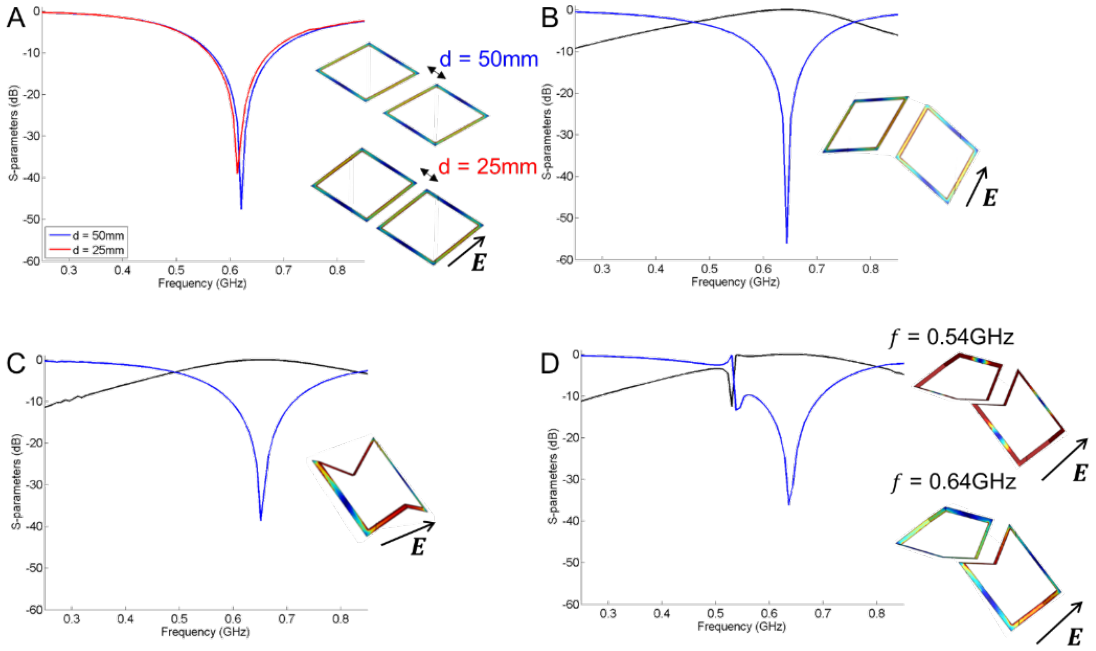

Figure 30: Case Studies to Investigate the Lower Resonance in Folded Square Loops

The potential of origami fold patterns as geometric reconfiguration mechanisms for EM resonances was investigated in this study. The results show that there are various mechanisms that cause changes in resonance characteristics of folded FSSs and motivate further investigation of a diverse combination of prints and folding patterns. In addition, the variety of resonance coupling and tuning capability demonstrated motivates the development of design tools to predict the optimal fold patterns and conductive patterns for specific EM performance criteria, similar to those developed for the actuator study.

8. Conclusions

The following points summarize the key accomplishments and significant conclusions that can be drawn from the current program:

1. A mechanical analysis tool based on truss elements was developed to analyze folded structures and to simulate folding of a flat structure. The analysis tool was integrated with an optimization method to find optimal origami crease patterns. This led to re-discovery of known action origami designs and discovery of new origami-based mechanism designs.
2. A mechanical analysis tool based on frame elements was developed to analyze structures involving complex deformations including folding, bending and twist. The structural analysis tool was combined with modal analysis and design optimization to find optimal origami patterns for in-plane compression.
3. Self-folding and programmable material systems were developed for tailored origami folding in Nafion and LCE systems. A remote actuation mechanism through joule heating was developed, using silver ink.
4. A 3D analysis tool based on brick elements was developed to predict the deformation of patterned LCE films. The analysis tool was integrated with a design optimization method to find optimal patterns for origami hinges and boxes.
5. Mechanically relevant metrics for folding were identified and quantified via a custom crease test apparatus, including residual fold angle, fold angle relaxation, dissipated mechanical energy, and size of the surface plastic zone.
6. Conventional FSSs, with conducting dipoles and loops, were folded to investigate the special reconfiguration of EM devices in the RF range. The performance sensitivity of EM devices proved their function tuning through origami a viable strategy.

These findings support our ongoing investigations of material behavior integration in the computational model and development of origami design methodology for folded artifacts with multiphysics function targets.

9. References

[1] M. Schenk and S. D. Guest, "Origami folding: A structural engineering approach," *Origami*[5]*,* pp. 291-304, 2011.

[2] K. Svanberg, "The method of moving asymptotes—a new method for structural optimization," *International journal for numerical methods in engineering,* vol. 24, pp. 359-373, 1987.

[3] M. P. Bendsøe and N. Kikuchi, "Generating optimal topologies in structural design using a homogenization method," *Computer methods in applied mechanics and engineering,* vol. 71, pp. 197-224, 1988.

[4] J. Shafer, *Origami Ooh La La! Action Origami for Performance and Play*: CreateSpace Independent Publishing Platform, US, 2010.

[5] L. A. Bowen, C. L. Grames, S. P. Magleby, L. L. Howell, and R. J. Lang, "A classification of action origami as systems of spherical mechanisms," *Journal of Mechanical Design,* vol. 135, p. 111008, 2013.

[6] J. Hetrick and S. Kota, "An energy formulation for parametric size and shape optimization of compliant mechanisms," *Journal of Mechanical Design,* vol. 121, pp. 229-234, 1999.

[7] T. Buhl, C. B. Pedersen, and O. Sigmund, "Stiffness design of geometrically nonlinear structures using topology optimization," *Structural and Multidisciplinary Optimization,* vol. 19, pp. 93-104, 2000.

[8] T. H. Ware, M. E. McConney, J. J. Wie, V. P. Tondiglia, and T. J. White, "Voxelated liquid crystal elastomers," *Science,* vol. 347, pp. 982-984, 2015.

[9] L. T. de Haan, A. P. Schenning, and D. J. Broer, "Programmed morphing of liquid crystal networks," *Polymer,* vol. 55, pp. 5885-5896, 2014.

[10] C. Modes, M. Warner, C. Sánchez-Somolinos, L. De Haan, and D. Broer, "Mechanical frustration and spontaneous polygonal folding in active nematic sheets," *Physical Review E,* vol. 86, p. 060701, 2012.

[11] L. T. de Haan, C. Sánchez-Somolinos, C. M. Bastiaansen, A. P. Schenning, and D. J. Broer, "Engineering of complex order and the macroscopic deformation of liquid crystal polymer networks," *Angewandte Chemie International Edition,* vol. 51, pp. 12469-12472, 2012.

[12] Kang, H., Park, J. S., Sohn, E. H., Kang, D., Rosenblatt, C., & Lee, J. C.. "Polyimide blend alignment layers for control of liquid crystal pretilt angle through baking". Polymer, 50(22), 5220-5227, 2009.

APPENDIX A: In-house Activities

Personnel:

Air Force

Name	Directorate	Degree	Discipline	Involvement (PY)
James Joo	RQ	PhD	Mechanical Eng.	0.2
Greg Reich	RQ	PhD	Aerospace Eng.	0.1
Phil Buskohl	RX	PhD	Theoretical Mechanics	0.4
Michael Durstock	RX	PhD	Materials Science	0.1
Loon-Seng Tan	RX	PhD	Chemistry	0.1
Richard Vaia	RX	PhD	Materials Science	0.1
Tim White	RX	PhD	Materials Science	0.1

On-Site Contractors

Name	Degree	Discipline	Involvement (PY)
Andrew Abbott	MS	Materials Eng.	1.0
Giorgio Bazzan	PhD	Chemistry	1.0
Kazuko Fuchi	PhD	Mechanical Eng.	1.0
Ryan Kohlmeyer	PhD	Chemistry	0.1
Jared Needle	BA	Mathematics	1.0
Taylor Ware	PhD	Materials Science	0.5
JJ Wie	PhD	Chemical Eng.	0.2
Michael Kuhn	BSME	Mechanical Eng.	0.5

APPENDIX B: Outreach, Community Leadership by LRIR Personnel

1. White, T.J. Organizer, Shape Programmable Materials Symposium, MRS Fall Meeting, November 29 – December 4, 2015, Boston, MA.
2. Joo. J. Co-Organizer, Symposium on Origami-Based Engineering Design, ASME International Design Engineering Technical Conference (IDETC), 2-5 August 2015 Boston, MA.
3. Vaia, R.A. Organizer, Symposium "Origami: Where Art, Devices and Structures Merge," SPIE DSS15 Micro-Nanotechnology Sensors, Systems, and Applications Conference, April 20-24, 2015.
4. Fuchi, K and Buskohl, PR. Organizers - Origami outreach session, Dayton Regional STEM School, June 4, 2015.
5. Joo. J. Co-Organizer, Symposium on Origami-Based Engineering Design, ASME International Design Engineering Technical Conference (IDETC), 17-20 August 2014 Buffalo, NY.
6. Fuchi, K. Guest Speaker, Educational Outreach, Workshop on Aerospace Systems and Origami at the Dayton Regional Stem School, June 6, 2014.
7. White, T. Co-Organizer, Shape Programmable Materials Symposium at the 2014 MRS Spring Meeting, 20-24 April 2014, San Francisco, CA.
8. Fuchi, K. Course Instructor, EGR 7040 Design Optimization at Wright State University, Fall 2014.
9. Joo, J. Co-Organizer, Symposium on Origami-Based Engineering Design, ASME International Design Engineering Technical Conference (IDETC), 4-7 August 2013 Portland, OR.
10. AFRL Team, Initial ODESSEI Origami Workshop, Dayton, OH, January 2013.
11. AFRL site visits and student exchange from ODESSEI teams:
    - Michael Dickey, "Externally-Triggered Origami of Responsive Polymer Sheets," April 2015, NC State
    - Richard Malak, "Synthesizing Complex Structures from Programmable Self-Folding Sheets," April 2015, TA&M
    - Manos Tentzeris "Inkjet-Printed Nanotechnology-enabled RFID, Internet of Things" and "Zero-Power" Wireless Sensor Nodes," June 2014, GT
    - Stavros Georgakopoulos, "Origami Reconfigurable Antennas," April 2014, FIU
    - Darren Hartl, "Analysis and Design of Functionally Optimized SMA-Based Reconfigurable Structures," May 2014, TA&M;
    - Spencer Magleby, "Origami-Inspired Design of Mechanical Systems," June, 2014, BYU
    - Student Exchange: John Gibson, EE Graduate Student (FIU, Georgakopoulos Lab) May-August 2014.

APPENDIX C: Publications, Presentations

Refereed Publications:

1. *Fuchi, K, *Ware, TH, Buskohl, PR, Reich, GW, Vaia, RA, White, TJ, Joo, JJ. Topology optimization for the design of folding liquid crystal elastomer actuators. **Soft Matter** 2015, 11, 7288 - 7295
2. Fuchi, K, Buskohl, PR, Bazzan, G, Durstock, MF, Reich, GW, Vaia, RA, Joo, JJ. Origami actuator design and networking through crease pattern design via topology optimization. **Journal of Mechanical Design** 2015 DOI:10.1115/1.4030876
3. Fuchi, K, Buskohl, PR, Bazzan, G, Durstock, MF, Reich, GW, Vaia, RA, Joo, JJ. Design optimization and challenges of large folding origami structures. **Proceedings of the ASME International Design, Engineering Technical Conference**, Boston, MA, August 2-5, 2015 **(recommended for *ASME Journal of Mechanisms and Robotics* submission)**
4. Kohlmeyer, R.R., Buskohl, P.R., Deneault, J.R., Durstock, M.F., Vaia, R.A., Chen, J. Shape reprogrammable polymers: encoding, erasing, and re-encoding. **Advanced Materials** 2014, 26.48 (2014): 8114-8119 **(cover)**
5. Wie, Jeong Jae; Wang, David H.; Lee, Kyung Min; Tan, Loon-Seng; White, Timothy J. "Molecular Engineering of Azobenzene-Functionalized Polyimides to Enhance Both Photomechanical Work and Motion" **Chemistry of Materials** 26.18 (2014): 5223-5230 (joint with LRIR 09RX06COR: PI Tan, PM: C. Lee)
6. Jeong Jae Wie, David H. Wang, Vincent P. Tondiglia, Nelson V. Tabiryan, Rafael O. Vergara-Toloza, Loon-Seng Tan, and Timothy J. White, "Photopiezoelectric Composites of Azobenzene-Functionalized Polyimides and Polyvinylidene Fluoride", **Macromolecular Rapid Communications**, 35.24 (2014): 2050-2056. (joint with LRIR 09RX06COR: PI Tan, PM: C. Lee)
7. Fuchi, K., Buskohl, P.R., Joo, J.J., Reich, G.W, Vaia, R.A. Topology optimization for design of origami-based active mechanisms. **Proceedings of the ASME International Design Engineering Technical Conference**, Buffalo, NY, August 17-20, 2014
8. Fuchi, K., Buskohl, P.R., Ware, T., Vaia, R.A., White, T.J., Reich, G.W, Joo, J.J. Inverse design of LCN films for origami applications using topology optimization. **Proceedings of the Smart Material, Adaptive Structures, and Intelligent Systems Meeting**, Newport, RI, Sept. 8-10, 2014
9. Abbott, A.C., Buskohl, P.R., Joo, J.J., Reich, G.W., Vaia, R.A. Characterization of creases in polymers for adaptive origami structures. **Proceedings of the Smart Material, Adaptive Structures, and Intelligent Systems Meeting**, Newport, RI, Sept. 8-10, 2014
10. Fuchi, K., Buskohl, P.R., Joo, J.J., Reich, G.W., Vaia, R.A. Numerical analysis of origami structures through modified frame elements. **Proceedings of the 6th International meeting on Origami in Science, Mathematics and Education**, August 10-13, 2014, Tokyo, Japan **(included as chapter in upcoming *Origami*^{6} book)**
11. Fuchi, K., Buskohl, P.R., Bazzan, G., Durstock, M.J., Reich, G.W., Vaia, R.A., Joo, J.J. Design Challenges of Origami-based Mechanisms with Sequenced Folding", **Journal of Mechanisms and Robotics**, 2015 (in press).

Non-Refereed Conference Proceedings:

1. Fuchi, K., Buskohl, P.R., Joo, J.J., Reich, G.W., Vaia, R.A. Resonance tuning of RF devices through origami folding. **Proceedings of the 20th International Conference on Composite Materials**, Copenhagen, Denmark, July 19-24, 2015

2. Buskohl, P.R., Fuchi, K., Reich, G.W., Joo, J.J., Vaia, R.A., Design tools for adaptive origami devices. **Proceedings of the Defense and Security. International Society for Optics and Photonics**, Baltimore, MD, April 20-24, 2015

Code Distributions:

OMTO v1.0 – Origami Mechanism Topology Optimizer v1.0, Available at Matlab Central: http://www.mathworks.com/matlabcentral/fileexchange/51811-origami-mechanism-topology-optimizer--omto-, **50+ downloads**

OMTO v1.1n - Origami Mechanism Topology Optimizer v1.1n, (programmer version) Available at Matlab Central: http://www.mathworks.com/matlabcentral/fileexchange/53037-origami-mechanism-topology-optimizer--omto--ver-1-1n, **20+ downloads**

Patents:

1. Loon-Seng Tan and David H. Wang, "Origami-inspired Fabrication of HighTemperature Shape Memory Polyimides," Provisional patent application #AFD1482 (filed on May 1, 2015) (joint with LRIR **09RX06COR**: PI Tan, PM: C. Lee).
2. Loon-Seng Tan and David H. Wang, "Multifunctional Crosslinkers for Shape-Memory Polyimides, Polyamides and Poly (amide-imides) and Methods of Making the same," U. S. Patent 8,962,890 (24-Feb-15). (joint with LRIR **09RX06COR**: PI Tan, PM: C. Lee)
3. Loon-Seng Tan, David H. Wang, Hilmar Koerner, and Richard Vaia, "Cross-Linked Aromatic Polyimides and Methods of Making the Same", U. S. Patent 8,791,227 (issued Jul 29, 2014) (joint with LRIR **09RX06COR**: PI Tan, PM: C. Lee)
4. Loon-Seng Tan, David H. Wang, Kyungmin Lee, and Timothy J. White "Azobenzene-Containing glassy Polyimides capable of photo-induced large-angle bending," U. S. Patent 8,785,589 (issued Jul 22, 2014) (joint with LRIR **09RX06COR**: PI Tan, PM: C. Lee)

Presentations (*Invited/Keynote) (25 + talks, 11 Invited):

1. *Reich, GW. "Design of origami structures and mechanisms for aerospace applications". Proceedings of the Smart Material, Adaptive Structures, and Intelligent Systems Meeting Colorado Spring, CO, Sept 21-23, 2015
2. Fuchi, K, Buskohl, PR, Joo, JJ, Reich, GW, Vaia, RA. "Design optimization of origami structures with coupled mechanics and electromagnetic analysis". Proceedings of the Smart Material, Adaptive Structures, and Intelligent Systems Meeting, Colorado Spring, CO, Sept 21-23, 2015
3. Fuchi, K, Buskohl, PR, Bazzan, G, Durstock, MF, Reich, GW, Vaia, RA, Joo, JJ. "Design optimization and challenges of large folding origami structures". Proceedings of the ASME International Design, Engineering Technical Conference, Boston, MA, August 2-5, 2015
4. Fuchi, K, Buskohl, PR, Joo, JJ, Reich, GW, Vaia, RA. "Resonance tuning of RF devices through origami folding". Proceedings of the 20th International Conference on Composite Materials, Copenhagen, Denmark, July 19-24, 2015
5. *Buskohl, PR. "Design tools for functional reconfiguration of liquid crystal elastomers" .Technical Interchange Meeting: Multiscale Characterization of Advanced Materials, Dayton, OH. June 29, 2015

6. Tan, L.-S.; Wang, D.H.; Koerner, H.; White, T.J.; Vaia, R.A. "Thermally activated shape-memory polyimides for origami-inspired objects in hot environment." 2015 European Polymer Congress, Dresden, Germany, June 21-26, 2015.
7. Buskohl, PR, Fuchi, K, Bazzan, G, Durstock, MF, Joo, JJ, Reich, GW, Vaia, RA. Design tools for adaptive origami devices" Proceedings of the Defense and Security. International Society for Optics and Photonics, Baltimore, MD, April 20-24, 2015
8. Buskohl, PR, Fuchi, K, Bazzan, G, Joo, JJ, Reich, GW, Vaia, RA. "Optimization of actuating origami networks". Proceedings of the American Physical Society Meeting, San Antonio, Mar. 2-6, 2015
9. *Vaia, RA. "Adaptive origami design tools for flexible hybrid electronics". Flexible and Printed Electronics Conference, Monterey, CA. Feb 23-26, 2015
10. *Buskohl, PR, "Design of Origami-based Materials: An Optimization Approach". NSF Workshop on Origami Design for Integration of Self-assembling Systems for Engineering Innovation (ODISSEI), Miami, FL, Jan 2015
11. *Abbott, A.C., Buskohl, P.R., Joo, J.J., Reich, G.W., Vaia, R.A. "Characterization of Creases in Polymers for Adaptive Origami Structures". Proceedings of the Society for the Advancement of Material and Process Engineering (SAMPE) student competition, Orlando, FL, Oct. 13-16, 2014. **(2nd Place Award, National Master's Division)**
12. *Reich, G.W. Panel discussion on origami engineering, ASME 2014 Conference on Smart Materials, Adaptive Structures and Intelligent Systems (SMASIS) 8-10, Sept. 2014. Newport, RI
13. Fuchi,K., Ware, T., Buskohl, P.R., Vaia, R.A., White, T.J., Reich, G.W., Joo, J.J., "Inverse design of LCN films for origami applications using topology optimization," Conference on Smart Materials, Adaptive Structures and Intelligent Systems, Newport, RI, Sept. 9, 2014
14. Abbott, AC, Buskohl, PR, Joo, JJ, Reich, GW, Vaia, RA. "Characterization of Creases in Polymers for Adaptive Origami Structures" Conference on Smart Materials, Adaptive Structures and Intelligent Systems, Newport, RI, Sept. 9, 2014
15. *Buskohl, PR. "Origami Material Design: Crossroad of Art and Engineering." University of Cincinnati Materials Science Graduate Seminar Series, Cincinnati, OH, Aug. 29, 2014
16. Abbott, A.C. "Characterization of Creases in Polymers for Adaptive Origami Engineering," Master's Thesis Defense, University of Dayton, Dayton, OH, July 1, 2014
17. *Vaia et al. "Where art and technology meet: Origami for 3D adaptive devices," 2014 SPIE DDS: Micro/Nanotechnology, Baltimore, MD May 3-5, 2014
18. Abbott, A.C., Buskohl, P.R., Needle, J., Joo, J.J., Reich, G.W., Vaia, R.A. "The "Fold": Performance criteria for polymers used in adaptive origami structures," Proceedings of the Materials Research Society Meeting, San Francisco, CA, Apr 21-25, 2014
19. *Reich, GW, Vaia, RA, White, TJ, Joo, JJ, Durstock, MF, Tan, LS, "Adaptive Origami for Aerospace Systems," Proceedings of the Materials Research Society Meeting, San Francisco, CA, Apr 21-25, 2014
20. Buskohl, P.R., Fuchi, K., Joo, J.J., Reich, G.W, Vaia, R.A. "Exploiting the rigid-compliant origami transition to design adaptive actuators". Proceedings of the Materials Research Society Meeting, San Francisco, CA, Apr 21-25, 2014
21. Ware, T., Wie, J.J., McConney, M.E., White, T.J. "Optimization of materials chemistry of photoresponsive liquid crystal polymer networks," Proceedings of the Materials Research Society Meeting, San Francisco, CA, Apr 21-25, 2014

22. Abbott, AC, Buskohl, PR, Joo, JJ, Reich, GW, Vaia, RA. "Polymeric Crease Characterization Techniques and Performance Criteria for Adaptive Origami Structures". Midwest Society for the Advancement of Material and Process Engineering (SAMPE) Student Symposium, Kettering, OH, April 3, 2014. **(1st Place Award, Midwest Master's Division)**

23. Buskohl, PR, Bazzan, G, Abbott, AC, Durstock, MF, Vaia, RA. "Targeting fold stiffness to design enhanced origami structures". Proceedings of the American Physical Society Meeting, Denver, CO, Mar. 3-7, 2014

24. *Reich, G.W. Panel discussion on origami engineering , ASME 2013 Conference on Smart Materials, Adaptive Structures and Intelligent Systems (SMASIS) SnowBird UT, Sept 16-18, 2013

25. *Joo, J.J., et al. "Adaptive Origami: Aerospace Potential". NSF Workshop on Origami Design for Integration of Self-assembling Systems for Engineering Innovation (ODISSEI), Miami, FL, Feb 2013

List of Acronyms, Abbreviations, and Symbols

Acronym/ Abbreviation	Description
AFRL	Air Force Research Laboratory
AFOSR	Air Force Office of Scientific Research
FLEX	Flexible Electronic Materials and Devices Research Team
FE	Finite Element
LCE	Liquid Crystal Elastomers
EM	Electromagnetics
FSS	Frequency Selective Surface
RF	Radio Frequency